



**HAL**  
open science

## Transgressive-regressive cycles in saline lake margin oolites: paleogeographic implications (Priabonian, Vistrenque basin, SE France)

Nazim Semmani, François Fournier, Philippe Léonide, Monique Feist, Sarah Boularand, Jean Borgomano

### ► To cite this version:

Nazim Semmani, François Fournier, Philippe Léonide, Monique Feist, Sarah Boularand, et al.. Transgressive-regressive cycles in saline lake margin oolites: paleogeographic implications (Priabonian, Vistrenque basin, SE France). Bulletin de la Société Géologique de France, 2022, 193 (8), 10.1051/bsgf/2022012 . hal-03949866

**HAL Id: hal-03949866**

**<https://hal.science/hal-03949866>**

Submitted on 20 Jan 2023

**HAL** is a multi-disciplinary open access archive for the deposit and dissemination of scientific research documents, whether they are published or not. The documents may come from teaching and research institutions in France or abroad, or from public or private research centers.

L'archive ouverte pluridisciplinaire **HAL**, est destinée au dépôt et à la diffusion de documents scientifiques de niveau recherche, publiés ou non, émanant des établissements d'enseignement et de recherche français ou étrangers, des laboratoires publics ou privés.



Distributed under a Creative Commons Attribution 4.0 International License



27 result from increasingly positive freshwater-evaporation balance volume but from the  
28 combination of subsidence and outflow from neighbouring saline waterbodies. The Butte  
29 Iouton carbonate margin is part of a set of interconnected saline lakes, occupying continental  
30 basins from Languedoc and Rhodanian region during the Priabonian, with a siliciclastic-  
31 dominated sedimentation in the southern margin, sourced by erosion of Pyrenean reliefs, and a  
32 carbonate-dominated northern margin with significant oolitic sedimentation in high-energy  
33 nearshore area.

34 **Keywords:** lacustrine carbonates, oolite, saline lakes, paleogeography, Eocene.

35

## 36 **Résumé**

37 **Cycles de transgression-régression sur une marge oolithique de lac salin : implications**  
38 **paléogéographiques (Priabonien, Bassin de la Vistrenque, Sud-Est de la France)**

39 L'étude intégrée d'une butte-témoin de carbonates lacustres (Butte Iouton) a permis d'établir  
40 un modèle de dépôt détaillé d'une marge carbonatée oolithique de lac salin, de mettre en  
41 évidence des cycles de transgression-régression et d'apporter des éléments de reconstitution  
42 paléogéographique des bassins lacustres priaboniens du sud-est de la France. Un modèle de  
43 rampe carbonatée lacustre a été mis en évidence, présentant du pôle proximal au pôle distal : 1)  
44 un domaine interne à laminites microbiennes et wackestones à ostracodes et mollusques, 2) un  
45 domaine plus ouvert, d'énergie modérée à sédimentation granulaire péloïdale et 3) un  
46 environnement externe de plus haute énergie à accumulation d'ooïdes et de péloïdes. La  
47 sédimentation carbonatée de bordure de lac se produit principalement pendant des phases de  
48 transgression lacustre contrôlées par la subsidence alors que les surfaces d'émersion marquent  
49 des périodes de bilan hydrique déficitaire et d'assèchement du lac (régression forcée). Les  
50 signatures isotopiques (carbone et oxygène) des carbonates ainsi que les tendances d'évolution  
51 verticale de la salinité estimées par les assemblages de mollusques suggèrent que les

52 transgressions lacustres ne sont pas associées à un bilan hydrologique excédentaire, mais à des  
53 connexions avec des masses d'eau salées adjacentes dans un contexte subsident. Les sédiments  
54 carbonatés de la Butte Iouton se sont déposés sur les marges d'un système de lacs salins  
55 interconnectés de grande dimension, occupant différents sous-bassins du Languedoc et de la  
56 Vallée du Rhône. La marge sud de ce système lacustre était à sédimentation silicoclastique  
57 dominante, alimentée par l'érosion des reliefs pyrénéens, alors que la marge nord était  
58 carbonatée avec un développement significatif de corps oolithiques.

59

60 **Mots-clés:** carbonates lacustres, oolithe, lacs salins, paleogéographie, Eocène.

61

## 62 **1. Introduction**

63 The European Cenozoic Rift System (ECRIS) (Ziegler, 1992; Dèzes et al., 2004) is a NE-SW  
64 system of continental lake basins formed during the upper Eocene in the Alpine foreland. These  
65 basins are characterized by thick siliciclastic, carbonate and evaporite deposits (e.g. Rouchy,  
66 1997). In southeast France, the onset of saline lakes occurred as early as the early Priabonian in  
67 the Saint-Chaptes basin (Lettéron et al., 2018) and then developed on a larger scale during the  
68 middle to late Priabonian in the Alès (Lettéron et al., 2018), Issirac (Lettéron et al., 2017),  
69 Mormoiron-Carpentras (Triat and Truc, 1974; Truc, 1978), Manosque-Forcalquier (Lesueur,  
70 1991) basins and further north in the Valence graben (Dromart and Dumas, 1997) (Fig. 1A).  
71 Despite detailed studies on individual basins or connected lake systems (e.g. ASCI lake system:  
72 Lettéron et al., 2022; Apt-Manosque-Forcalquier lake system: Lesueur, 1991), there are still  
73 unresolved questions, debates and controversies on the paleogeography of western Europe  
74 during the late Eocene – lower Oligocene times, the origin of the salinity in the lakes and the  
75 connections between the lakes and the oceanic realm (e.g. Fontes et al., 1991; Rouchy, 1997;

76 Briot and Poidevin, 1998; Bodergat et al., 1999; Rouchy and Blanc-Valleron, 2009; Lettéron et  
77 al., 2017; 2018). For instance, Lettéron et al. (2017, 2018) found that the ASCI lacustrine  
78 system was connected to neighbouring saline water bodies whose location and source are not  
79 formally established. According to these authors, saline water feeding is presumably from the  
80 leaching of northern Triassic diapirs via Mormoiron-Carpentras throughs and/or marine domain  
81 through the Vistrenque area. The latter is poorly documented since the Paleogene deposits are  
82 almost entirely buried beneath the Rhône delta sediments.

83 Another major issue for the reconstruction of paleogeographic and tectonic evolution of  
84 Paleogene basins from southeast France is the availability and quality of chronostratigraphic  
85 constraints (Séranne et al., 2021). East of the Nîmes fault, the Cenozoic Vistrenque graben is  
86 known only through subsurface studies and has been assigned to the Oligocene Gulf of Lion  
87 margin (Valette and Benedicto, 1995; Benedicto et al., 1996), while Cavalier (1984) suggested  
88 that the Vistrenque graben initiated during the Priabonian coevally with the neighbouring  
89 Languedoc basins such as the north-Montpellier, Sommières, Saint-Chaptes, Ales and Issirac  
90 basins (Séranne et al., 2021; Lettéron et al., 2022). To date, the paucity of chronostratigraphic  
91 data from the basal filling of the graben (*Série grise* siliciclastic unit, e.g. Valette and Benedicto,  
92 1995) does not allow this hypothesis to be validated. However, the northern part of the basin  
93 offers the possibility to study on outcrops carbonate successions assumed to be upper Eocene  
94 in age (Roman, 1910) and thus provides clues to address the question.

95 In the present work, we carry out a detailed petrographic, sedimentological and geochemical  
96 analysis of a carbonate succession which outcrops on a residual hill (Butte Iouton, Beaucaire)  
97 located east of the Nîmes fault on the northern margin of the Vistrenque graben and that is  
98 characterized by the dominance of oolitic deposits (Fig. 1A, 3A). The main objectives of this  
99 study are 1) to document the existence of a salt lake carbonate sedimentation during the  
100 Priabonian in the north of the Vistrenque basin and provide new constraints to the

101 chronostratigraphic framework 2) to reconstruct the depositional environments for a Cenozoic  
102 oolitic saline lake margin 3) to discuss the control of tectonics and paleohydrological changes  
103 onto the vertical facies stacking pattern and depositional sequence development and 4) to  
104 provide new insights into the paleogeography of the southeast France by investigating the  
105 possible relationships between the saline lake basins of the ECRIS.

## 106 **2. Geological setting**

### 107 **2.1. The Vistrenque Cenozoic basin: regional tectonic setting and stratigraphy**

108 The Vistrenque basin is a NE-SW trending Cenozoic basin located in the western part of the  
109 Camargue region (SE France). The basin extends over 50\*30 Km<sup>2</sup> and is assumed to be the  
110 deepest Cenozoic basin in the SE of France ([Benedicto et al., 1996](#)), it is linked to the Northeast  
111 with the Pujaut trough and is separated from the neighbouring Vaccarès (Petit-Rhône) basin by  
112 the Albaron structural high ([Fig. 1A](#)).

113 The Nîmes fault is a major low angle-ramp that bounds the Vistrenque and Pujaut basins to the  
114 NW and was active during the Oligo-Aquitainian rifting of the Gulf of Lion margin that  
115 preceded the oceanic accretion in the Liguro-Provençal basin during the Burdigalian ([Gorini et](#)  
116 [al., 1993](#); [Séranne et al., 1995](#); [Valette and Benedicto, 1995](#); [Benedicto et al., 1996](#)).

117 Prior to the Oligo-Miocene rifting, strike-slip deformation regime led to the development of  
118 many continental sedimentary basins (e.g. Alès–Saint-Chartes–Issirac basin, [Lettéron et al.,](#)  
119 [2022](#)) during the Priabonian (late Eocene) in Languedoc area within a NE trending sinistral  
120 strike-slip shear zone, located between the Cévennes and Nîmes faults ([Séranne et al., 2021](#)).

121 The Eocene and Oligocene basins of the Languedoc area have well constrained  
122 chronostratigraphic frameworks and their depositional and structural settings are well  
123 documented ([Benedicto et al., 1996](#); [Séranne et al., 2021](#); [Lettéron et al., 2022](#)). The Nîmes and  
124 Cévennes sinistral strike-slip faults have accommodated simultaneously the E-W extension of

125 the Western European rifting in the north and the Pyrenean compression from the south  
126 (Séranne et al., 2021). In the Camargue region located southern to the Languedoc, Eocene  
127 deposits are only known from the Jonquières high (Fig. 1A), and no evidence can be provided  
128 to confirm the presence of upper Eocene deposits in the Camargue basins (e.g. Vistrenque  
129 basin) since their chronostratigraphic framework is not constrained (Benedicto et al., 1996).

130 Stratigraphically, the Eocene (?) to Aquitanian sedimentary succession of the Vistrenque basin  
131 exceeds 3000 m in thickness and is subdivided in the depocentre of the basin into three main  
132 units, from bottom to top: *Série grise* (more than 2000 m thick), *Série Rouge* (~ 200 m) and  
133 *Série Calcaréo-salifère* (900 m) formations (Benedicto, et al., 1996). The lowermost *Série grise*  
134 unit consists mainly of deep-lake non-fossiliferous mixed siliciclastic-carbonate detrital  
135 sediments and their attribution to the beginning of the Oligo-Miocene gulf of Lion rifting  
136 (Benedicto, 1996) or to the late Eocene development of continental basins is an open question.  
137 The upper *Série Calcaréo-Salifère* unit is made essentially of evaporite deposits that were  
138 assigned to the Upper Oligocene (Valette, 1991). According to Cavelier (1984), the similarity  
139 of the sedimentation pattern between the Languedoc grabens and Vistrenque basin (i.e.  
140 dominant siliciclastic sedimentation to south and carbonate lacustrine margin to the north)  
141 would suggest that the deposition of the lowermost *Série grise* unit or at least the basal intervals  
142 of this unit was coeval with the widespread Priabonian continental sedimentation in the Issirac,  
143 Alès, Saint-Chaptes and Sommières basins.

## 144 **2.2. The Jonquières high: stratigraphy of the Priabonian lacustrine margin**

145 The Jonquières high is about 5-6 km wide and represents a NE-SW horst structure bordering  
146 the Vistrenque basin to the north and located southeast to the Pujaut through and northwest to  
147 the Tarascon trough (Fig. 1A). The high is constituted essentially of the Lower Cretaceous  
148 substratum; the Eocene to Miocene cover is limited to a few small residual hills between the  
149 villages of Comps and Beaucaire (Fig. 1B). Resting on the Hauterivian marine limestones and

150 marly limestones, the Eocene deposits from these hills (e.g. butte Iouton) consist essentially of  
151 a ~30 m thick lacustrine limestone succession resting on variegated clays and silts (about 20 m  
152 thick interval) attributed by [Pellat and Allard \(1895\)](#) to the early Eocene on the basis of regional  
153 facies analogy without any paleontological evidence. These Eocene lacustrine limestones are  
154 unconformably overlain by Burdigalian (early Miocene) transgressive coralline algal marine  
155 limestones ([Pellat and Allard, 1895](#); [Roman, 1903](#)) ([Fig. 1C](#)).

156 The lacustrine limestones from Butte Iouton include oolitic intervals that have been exploited  
157 since the Middle Ages as a statuary stone ([Dumas, 1876](#)). They yielded a rich molluscan fauna  
158 that has attracted the attention of geologists since the first half of the 19th century ([de Roys,](#)  
159 [1846](#)). The first detailed section of the Butte Iouton hill was carried out by [Pellat and Allard](#)  
160 ([1895](#)) who identified 9 main fossiliferous carbonate layers and mentioned a preliminary list of  
161 fossil molluscs. [Roman \(1910\)](#) took charge of the detailed study of fossil molluscs from the  
162 regional “Sannoisian” formations and has drawn up a comprehensive inventory that consists of  
163 30 taxa including eight holotypes (hosted in the collections of the University of Lyon) of  
164 gastropod species.

### 165 **3. Material and methods**

166 The 50m-thick Cenozoic succession of the Butte Iouton hill has been mapped ([Fig. 1B](#)). Most  
167 of the carbonate section is quarried on the western flank of the hill (see location in [Fig. 1C](#)) thus  
168 enabling a continuous and detailed observation of the rock succession. Data on sedimentary  
169 structures, depositional textures, biological content, and diagenetic features are compiled in the  
170 detailed sedimentary log ([Fig. 2](#)).

#### 171 *Depositional facies and petrographic characterization*

172 A total of 28 thin sections have been prepared to perform detailed microfacies characterization  
173 and to determine the petrographic features of the grains using a conventional transmitted

174 polarized light microscope. Carbonate depositional facies have been defined on both  
175 macroscopic descriptions and microscopic observations using the Dunham classification of  
176 carbonates (Dunham, 1962) expanded by Embry and Klovan (1971). Point-counting (300  
177 points) performed with the JMicroVision software allows to quantify the allochem proportions  
178 in thin sections (Roduit, 2007). SEM observations conducted at Pôle PRATIM (Plateforme de  
179 Recherche Analytique Technologique et Imagerie, Aix-Marseille University, FSCM) using a  
180 Philips XL30 ESEM (environmental scanning electron microscope) enable to investigate in  
181 more detail the internal microstructure of some carbonate grains.

### 182 ***Biological assemblages and chronostratigraphic framework***

183 Particular attention was paid to the examination of the quarry's fossiliferous layers to determine  
184 the fossil assemblages, namely the molluscs (gastropods and bivalves) and the remains of  
185 characean algae (Fig. 3). Molluscan assemblages provide key indication for paleoecological  
186 reconstructions (e.g. Lettéron et al., 2017) and contribute to a lesser extent to constrain the  
187 chronostratigraphic framework (Cavelier, 1984). Charophyte gyrogonites constitute an  
188 essential tool to better constrain the age of the deposition of fresh and brackish water carbonates  
189 and will therefore be used for the biostratigraphic review of the studied succession from the  
190 butte Iouton hill. Molluscan shells and charophyte gyrogonites are often well preserved and are  
191 easily extracted. In few horizons, the shells are totally dissolved and only the external moulds  
192 remain. Casts have been made by injecting silicone resin into the moulds and the resulting casts  
193 allow a detailed examination of the external ornamentation of the molluscan shell casts. The  
194 identification of the molluscan taxa is carried out in accordance with the diagnoses documented  
195 in Fontannes (1884) and in Roman (1910). The fossil collection of Pierre de Brun, hosted in the  
196 Museum of Paleontology of the Aix-Marseille University, that catalogues most of the molluscs  
197 found in the butte Iouton have been also consulted.

198 The chronostratigraphic framework of the butte Iouton limestones has been therefore  
199 established using: (1) characean gyrogonites and (2) key molluscan taxa with significant  
200 stratigraphic value.

### 201 *Carbon and oxygen stable isotopes*

202 A total of 58 powdered samples (average spacing = 50 cm) were extracted from the limestones  
203 using a Dremel micro-drill tool. Bulk-rock stable carbon and oxygen isotope analyses were  
204 performed at the GeoZentrum Nordbayern department, Friedrich-Alexander-Universität  
205 Erlangen-Nürnberg (Germany) in order to detect potential diagenetic overprints (e.g.  
206 pedogenesis at exposure surfaces) and/or to provide insights into lake paleohydrology. The  
207 analysis technique employed consists in the reaction of the powders with 100% phosphoric acid  
208 at 70°C using a Gasbench II connected to a Thermo Fisher Scientific DELTA V Plus mass  
209 spectrometer. All values are reported in per mil relative to V-PDB. Reproducibility and  
210 accuracy were monitored by replicate analysis of laboratory standards calibrated by assigning  
211  $\delta^{13}\text{C}$  values of +1.95‰ to NBS19 and -47.3‰ to IAEA-CO9 and  $\delta^{18}\text{O}$  values of -2.20‰ to  
212 NBS19 and -23.2‰ to NBS18. Reproducibility for  $\delta^{13}\text{C}$  and  $\delta^{18}\text{O}$  was  $\pm 0.04$  and  $\pm 0.03$  (1  
213 standard deviation), respectively.

## 214 **4. Results and interpretations**

### 215 **4.1. Biostratigraphy**

216 The Butte Iouton quarry yields two taxa from the genus *Gyrogona* and some specimens are  
217 catalogued in the collections of the University of Montpellier under the number CF.3088.

218 a. *Gyrogona caelata* Ried and Groves, 1921 ([Fig. 4A](#))

219 This species is largely dominant in the charophyte assemblage. The general morphology as well  
220 as the dimensions of the examined samples are consistent with the definition given by [Grambast](#)

221 and Grambast-Fessard (1981). *G. caelata* is widespread in the European area and occurs within  
222 the charophytes biozones ranging from *Maedleriella embergeri* zone to *Stephanochara*  
223 *vectensis* zone (Riveline et al., 1996). These biozones encompass the upper Lutetian –  
224 Priabonian interval.

225 b. *Gyrogona* aff. *lemanii capitata* Grambast and Grambast-Fressard, 1981 (Fig. 4B)

226 This species is uncommon in the butte Iouton deposit and only a couple of specimens have been  
227 identified. The specimens meet the morphological criteria given by Grambast and Grambast-  
228 Fessard (1981) although their dimensions are found to be slightly smaller. This taxon is reported  
229 from many areas in Western Europe, such as the Paris Basin, Campbon Basin (southern  
230 Brittany), Upper Rhine Basin (Bouxwiller site) and southwestern Languedoc (Causse-et-  
231 Veyran site) (Riveline, 1986). *G. lemanii capitata* appears, together with the whole species of  
232 the genus *Gyrogona*, within the *Maedleriella embergeri* biozone and has a lesser range than *G.*  
233 *caelata* (Riveline et al., 1996). The former extends only up to the *Psilochara repanda* biozone,  
234 thus suggesting an age ranging from the Lutetian to the upper Bartonian. The difference in  
235 dimensions with the holotype raises uncertainties about the taxonomic attribution of the two  
236 specimens to *G. lemanii capitata*, hence the insertion of the complement aff. (*species affinis*).  
237 The insufficient amount of material makes it difficult any attempt to define a new species.  
238 Because of such a taxonomic uncertainty, these two specimens were not considered for  
239 constraining biostratigraphic ages.

240 The molluscan taxa identified on the butte Iouton outcrops are illustrated in Figure 4 and fall  
241 within the list of taxa compiled by Roman (1910) (Fig. 4C-K). Out of a total of the 30 molluscan  
242 taxa described by the same author in this site, 15 species are also documented from the  
243 molluscan associations of the middle to upper Priabonian successions from the Alès and Issirac  
244 basins (Fontannes, 1884; Lettéron et al., 2017). Among the mollusc taxa of the butte Iouton,  
245 some fossils are considered to have a reliable regional stratigraphic value and are therefore used

246 as key-stratigraphic markers in continental settings (Cavelier et al., 1984; Fauré, 2007). For  
247 instance, *Nystia plicata* (d'Archiac & Verneuil, 1855) extends from the late Priabonian to the  
248 Rupelian while *Viviparus soricinensis* (Noulet) has a much wider range since it is known from  
249 middle Priabonian up to Rupelian deposits. However, the bivalve *Polymesoda dumasi* (M. de  
250 Serres, 1827) has a narrow range since it occurs only from the middle to upper Priabonian and  
251 has never been reported in the Oligocene successions. Along with the previously discussed  
252 stratigraphic implications of the charophyte flora, the molluscan assemblage especially the  
253 occurrence of the taxa *N. plicata* and *P. dumasi* provides strong evidence to assign a late  
254 Priabonian age to the Butte Iouton limestones.

#### 255 **4.2. Carbonate petrography and diagenetic features**

256 Petrography and SEM observations of thin sections from the butte Iouton limestones help to  
257 identify five grain types, namely ooids, peloids, aggregate grains, reworked sparitic crusts and  
258 miscellaneous skeletal grains including molluscans (both bivalves and gastropods) and  
259 ostracods, and charophyte remains.

260 Ooids are the dominant grain type and are generally small, averaging 300 microns in diameter  
261 (medium sand) (Fig. 5A, 6A-B). These small ooids display various cortex fabrics: thin cortices  
262 are found in superficial ooids while radial fibrous or concentric micritic cortices define radiaxial  
263 (Fig. 5A-B) and micritized ooids (Fig. 5C-D) respectively. The ooids have either peloid,  
264 bioclast or fine quartz grain nuclei and show different stages of micritization obliterating the  
265 original microstructure. Other coated grains include coarse ooids and/or oncoids (=coated  
266 grains whose cortex is formed by cyanobacterial laminae) (Fig. 6G), their sizes range between  
267 600 microns and may reach up to 2 mm and most of them display concentric laminae cortices.

268 Peloids are frequent in the butte Iouton limestones and show various shapes and sizes (Fig. 5A-  
269 6E-F). Peloids are in general sub-rounded to elongated, range between 80 and 200 microns in

270 size and display dark and homogeneous micritic internal structure. Aggregate grains from the  
271 butte Iouton section are very irregular in shape and are recognized based on the characteristic  
272 lobate to rounded outlines (Fig. 6E). These aggregate grains have a wide range of sizes from  
273 0.5 mm to several mm and the original separate grains may either be peloids or micritized ooids;  
274 their smooth outlines allow to consider them as lumps according to the description provided by  
275 Tucker and Wright (1990). Reworked sparitic crusts are flattened and are thin sheets formed by  
276 calcite crystals arranged side by side. The sparry crystals are equigranular, dogteeth shaped,  
277 and each is between 40 and 50  $\mu\text{m}$  in size (Fig. 7F). Calcite crystals line up in one or more rows  
278 and this may reflect single or multiple generations of crystal growth from an initial surface,  
279 possibly a microbial film and have been reworked and re-deposited without any particular  
280 orientation.

281 The molluscs from the butte Iouton limestones consist mainly of freshwater to oligo-mesohaline  
282 taxa. Gastropods and bivalves may be found in the form of entirely micritized calcitic shells  
283 (Fig. 6E-F) or recognized by their external moulds if they are completely dissolved, especially  
284 in case of formerly aragonitic shells (Fig. 7A, 7D, 7G-H). Ostracods (Fig. 7G) and characean  
285 gyrogonites (Fig. 8C) are preserved owing to their original calcite mineralogy.

286 The main diagenetic processes observed are: a) compaction (ooids, shells, characean remains),  
287 b) micritization of molluscan shells and ooid cortices, c) selective mouldic dissolution of  
288 aragonite grains (mainly molluscs), d) cementation (calcite spar: Fig. 8E), e) pedogenesis (soil  
289 formation, brecciation), and f) calcite pseudomorphs after gypsum (Fig. 8E).

290 Petrographic observations show preferential dissolution of the aragonite shells of molluscs and  
291 the preservation of the ooids cortices that may point to different original mineralogies of these  
292 grains, while some samples display strong micritization of both molluscan shells and ooids. The  
293 original mineralogy of the ooids is difficult to establish since both radiaxial and micritized  
294 layers can coexist and since petrographic observations show evidences of severe neomorphic

295 processes. The mineralogy of ooids and their fabric, in particular those formed in freshwater  
296 and extreme environments is still a matter of debate (e.g. [Kahle, 1974](#); [Sandberg, 1975, 1980](#);  
297 [Swirydczuk and Wilkinson, 1979](#)).

### 298 **4.3. Depositional facies and paleoenvironmental interpretations**

299 Based on depositional texture (Dunham classification), sedimentary structures, biotic  
300 composition, and the petrographic character of the allochems, nine depositional facies have  
301 been defined and summarized in [Table 1](#).

#### 302 **F1A. Oolitic-peloidal grainstone**

303 This facies consists of moderately to well-sorted grainstones composed of a mixture of ooids  
304 and peloids in variable proportions: ooids (~ 300 microns in size) are dominant and their  
305 proportion ranges from 50% (bimodal distribution) to 95% (unimodal distribution) ([Fig. 6A-](#)  
306 [B](#)). Some ooids exhibit preserved superficial and radial internal structures although most of  
307 them are strongly micritized. The peloids are predominantly small and have different  
308 morphologies, their dimensions range between 100 and 200 microns; other allochems include  
309 few aggregate grains (<1%). Molluscan shells and fragments can accumulate in the form of  
310 fossiliferous gravelly lenses interbedded with the ooidal-peloidal sand levels ([Fig. 6C](#)). The  
311 gravelly lenses are about 10 cm thick and few metres wide, and most of the fossils are complete  
312 or slightly broken. The molluscan assemblage is dominated by *Melanopsis*, *Tarebia* and  
313 *Neritina*. Together with the peloidal grainstones (see description hereinafter), the oolitic-peloidal  
314 grainstones form subhorizontal beds with thicknesses varying from 2 m to 3 m ([Fig. 3B-6C](#)).  
315 Cross-stratifications are seldom visible on outcrop and when observed (e.g. [Fig. 6D](#)) they may  
316 form 10-50 cm height sets that are bounded at base and top by planar nearly horizontal surfaces  
317 (“planar cross-stratifications”). The scarce apparent paleocurrent directions measured on the  
318 quarry faces are toward the south-west.

319 **Interpretation:** The moderately to good sorting of these grainstones and the winnowing of the  
320 micrite suggest high energy depositional conditions. Though seldom observable, the occurrence  
321 of planar cross-stratifications within the oolitic beds may reflect sandwaves or dunes migration  
322 related to high energy currents (Dalrymple, 1992). Ooids are generally produced in shallow  
323 nearshore shoals subject to high hydrodynamic conditions and form very well sorted sediments.  
324 Thus, the mixture of ooids and peloids in F1A facies suggests deposition in the vicinity of these  
325 shoals where ooids are remobilized by waves and currents. In lacustrine environments, well  
326 sorted oolitic sediments are essentially reported from shallow lake margin shoreface (e.g.  
327 Williamson and Picard, 1974; Tānavsuu-Milkeviciene et al., 2017; Gallois et al., 2018;  
328 Deschamps et al., 2020) and foreshore settings (Swirydczuk et al., 1980; Milroy and Wright,  
329 2002). The relative scarcity of sedimentary structures in most oolitic beds may result from  
330 significant burrowing of a stable substrate in a low to moderate energy environment in  
331 backshoal setting as reported from shallow marine environments (Pomar et al., 2015). The  
332 molluscan-rich gravelly lenses are also indicative of moderate to high energy at least  
333 intermittently to make fossil accumulations possible. Gastropod *Tarebia* is known to thrive  
334 preferentially in oligo-mesohaline waters (e.g. Plaziat and Younis, 2005; Esu and Girotti, 2010;  
335 Miranda et al., 2010) while *Melanopsis* is mostly indicative of freshwater to oligohaline settings  
336 (Velasco et al., 2006). Plaziat and Younis (2005) found that smooth morphologies of  
337 *Melanopsis*, such as evidenced in Butte louton specimens, prefer brackish-water environments.  
338 The oolitic-peloidal grainstones and gravelly lenses are therefore interpreted to form within  
339 and/or at the vicinity of shallow nearshore oolitic shoals, in low to moderate salinity (from  
340 oligo- to mesohaline) and moderate to intermittently high energy waters.

#### 341 **F1B: Peloidal grainstone with scattered molluscs**

342 F1B facies consists of a moderately to well-sorted grainstones composed mainly of peloids with  
343 proportions ranging between 75% and 90% and molluscan shells (<20%) with few aggregate

344 grains and ooids (Fig. 6E). The peloids occur in a wide range of morphologies and are between  
345 0.05 and 0.2 mm in size. The aggregate grains (Fig. 6E) are large with dimensions comprised  
346 between 0.5 mm and few millimetres and are often lumps formed by peloids and few micritized  
347 ooids bound together by microbial cement. Gastropods are the dominant organisms found in  
348 these facies and their association is similar to that described previously from the oolitic-peloidal  
349 grainstones, among others *Melanopsis* and *Tarebia*: the shells are found to be entirely  
350 micritized. Together with the previously described oolitic-peloidal sands (F1A) and the gravelly  
351 fossiliferous lenses, these peloidal grainstones are organized into massive (2-3 m thick) and  
352 subhorizontal, structureless beds.

353 **Interpretation:** Like in the F1A facies, the lack of mud matrix and the good sorting of the  
354 grains suggest that F1B facies are deposited in moderate to high energy settings. In addition,  
355 the occurrence of F1B facies together with F1A facies and the presence of minor proportion of  
356 ooids in the peloidal sands strongly indicate nearby depositional environments. The good  
357 sorting and the low variation in shape of peloids suggest they are likely to be mostly produced  
358 by organisms (i.e., faecal pellets) like gastropods and ostracods. Molluscan-rich accumulations  
359 probably result from transportation and deposition of molluscan shells during higher energy  
360 episodes. Similarly to F1A, the molluscan assemblage indicates oligo-mesohaline shallow  
361 waters probably of less than 10 m in depth (e.g. [Lettéron et al., 2017](#) and references therein).  
362 Furthermore, the absence of subaerial exposure features within these facies indicates perennial  
363 lake conditions. Consequently, F1B facies is interpreted to form in the shallow parts of a  
364 perennial lake close to the oolitic shoals with moderate to high energy levels.

#### 365 **F1C: Oncoidal-oidal rich peloidal grainstone**

366 F1C facies is a peloidal grainstone comprising large proportions of oncoids and coarse ooids,  
367 and molluscan shells (Fig. 6F-G). This facies has been only encountered within centimetre to  
368 few centimetres thick lenses, interbedded within F1B peloidal grainstones at top of U2 and in

369 U4 cycle. Peloids are predominant (50%) and the coated grains (20-40%) consist either of  
370 coarse ooids (~ 600-900 microns) or oncoids (up to 2 mm in size), their grain distribution  
371 exhibits floating coarse grains in a peloidal matrix. The molluscan shells are less frequent and  
372 are strongly micritized.

373 **Interpretation:** The scarcity of mud matrix in these grainstones indicates at least intermittent  
374 water turbulence allowing the winnowing of fines. In addition, the poor sorting and the presence  
375 of coarse coated grains reflect sporadic high energy events such as fluvial floods. The peloids  
376 from F1C facies resemble those of F1B facies in which they are intercalated, and therefore may  
377 form in the same perennial shallow lake settings with moderate to high water energy. Oncoid-  
378 rich grainstones have been found to form as a result of fluvial overbank in lacustrine and  
379 floodplain environments ([Schäfer and Stapf, 1978](#); [Arenas et al., 2007](#); [Lettéron et al., 2018](#)),  
380 but are also common along the shoreline of various modern and ancient lakes (e.g. Plio-  
381 Pleistocene from Lake Turkana: [Hargrave et al., 2014](#); [Nutz et al., 2020](#); Lake Geneva: [Davaud  
382 and Girardclos, 2001](#)). Therefore, the F1C facies is interpreted to form in a shallow nearshore  
383 environment of a perennial lake, similar to that of F1B depositional environments, the oncoids  
384 perhaps deriving from the shoreline or from a nearby mouth of an oncoid-producing river.

385

#### 386 **F2A: Molluscan-rich peloidal packstone-grainstone**

387 This facies consists of limestones containing large amounts of small peloids mixed with  
388 frequent molluscs, few ostracods and scarce small ooids set in micrite to microspar matrix ([Fig.  
389 7A-7D](#)). The peloids are densely packed, irregular in shape and are very small (80-200 microns  
390 in size). The molluscan shells are dissolved, and the organisms are identified only from their  
391 external moulds, the biological association comprises mainly *Polymesoda*, *Hydrobia* and

392 *Tarebia* (Fig. 7B). These peloidal-dominated packstones are found in the form of decimetre  
393 thick beds and are devoid of sedimentary structures (Fig. 7C).

394 **Interpretation:** The occurrence but relative scarcity of micrite matrix suggests relatively calm  
395 environments but with transient periods of higher energy. The abundance of peloids in the  
396 matrix and their regular shape and comparable size (50-100  $\mu\text{m}$ ) may be interpreted as faecal  
397 pellets and likely results from the presence of abundant molluscan and crustacean communities.  
398 The molluscan assemblage dominated by *Polymesoda* and *Hydrobia* and *Tarebia* is indicative  
399 of warm, shallow and oligo-mesohaline waters (Daley, 1972; Morton, 1983, Fretter and  
400 Graham, 1978, Lett ron et al., 2017). Extant *Polymesoda* bivalves are found in a variety of  
401 variable salinity shallow environments (Reichenbacher et al. 2004; Harris et al., 2015) and their  
402 optimal depth is lower than 1 m (Tabb and Moore, 1971) even though these may be found at  
403 depths of 10 m (Morton, 1983; Lett ron et al., 2017). *Polymesoda* are found both valves  
404 connected thus indicating deposition in their living environment. Extant *Hydrobia acuta*  
405 *neglecta* are found in coastal lagoons where salinity ranges between 10 and 24‰ (Fretter and  
406 Graham, 1978). Thus, the biological community of F2A facies, particularly through the  
407 presence of *Hydrobia*, exhibits the greatest tolerance to salinity elevation compared to the  
408 freshwater to oligo-mesohaline gastropods and charophytes found in the overlying and  
409 underlying levels (F2B and F2D facies, see descriptive sections hereinafter). The lack of  
410 subaerial exposure features indicates deposition in perennial waters. The facies F2A is therefore  
411 interpreted to form in shallow, warm, and brackish lake with low to moderate water energy.

#### 412 **F2B: Characean-rich peloidal wackestone to packstone**

413 This facies consists of a mixture of densely packed peloids of very small size (50 - 100 microns)  
414 with frequent characean cortical cells, stems and gyrogonites, and numerous ostracods,  
415 occasional molluscs and few ooids (Fig. 7C-7E). The charophytes remains are preserved and  
416 are slightly compacted. Molluscan shells are either entirely leached or completely micritized

417 and their association is dominated by *Polymesoda*, *Tarebia* and hydrobids. F2B facies occurs  
418 in several centimetres to decimetre thick tabular to nearly horizontal beds and form together  
419 with F2A peloidal packstones an approximately 4 m high package of platelets limestones (Fig.  
420 7C).

421 **Interpretation:** The mud-supported texture results from the trapping of micrite and peloids and  
422 indicates low water energy which limits the winnowing of fine particles. The abundance of  
423 characean remains reflects the development of macrophyte meadows in shallow lake margin  
424 environments which act like a natural barrier against hydrodynamic energy. Charophytes  
425 colonize lacustrine substrates and may cover large areas but are limited by light penetration and  
426 their maximum depth does not exceed 12 m (Garcia, 1994; Garcia and Chivas, 2006) thus  
427 supporting the shallow water column during the deposition of the F2B facies. Charophytes  
428 thrive in freshwater lakes, but some taxa tolerate brackish waters and withstand changes in  
429 salinity (Garcia, 1994; Van Den Berg et al., 1998, Lettéron et al., 2017). In addition, the  
430 molluscan assemblages found in these wackestones indicate warm, shallow and fresh to oligo-  
431 mesohaline waters. Finally, the F2B facies reflects deposition within calcifying and non-  
432 calcifying charophyte meadows in shallow, freshwater to oligo-mesohaline lake settings.

#### 433 **F2C: Peloidal wackestone to packstone with calcitic rafts**

434 This facies occurs in decimetre tabular beds formed by densely packed peloids similar to those  
435 from facies F2A and F2B and comprises various proportions of crystalline flakes (calcitic rafts),  
436 few ostracods and scarce small gastropods and ooids (Fig. 7F). The peloids are very small (120-  
437 200 microns in size) and may be of faecal origin. Calcite rafts, described early as reworked  
438 sparitic crusts, are fragmented into pieces of various size (0.1 to 5 mm) or even as individual  
439 spar crystal. Gastropod shells are entirely leached. Faunal content is poor and molluscan  
440 assemblage is dominated by *Polymesoda* and *Tarebia*. These facies are found close to the F2A  
441 and F2B tabular beds and arranged together within the platelets limestones package.

442 **Interpretation:** The abundance of mud matrix in these facies suggests deposition in low-energy  
443 areas. However, the breakage of the calcite rafts and the abundance of peloids indicate  
444 intermittent hydrodynamic conditions. Features resembling those crystalline flakes are  
445 documented in the literature and many hypotheses have been considered to explain their origin.  
446 Many authors described these structures in various depositional settings and referred to them  
447 as calcite rafts, paper thin rafts and floating mats (see review in [Lettéron et al., 2018](#) and  
448 references therein). The abundance of peloids may indicate abundant gastropods and crustacean  
449 communities. The presence of small gastropods is indicative of shallow lake conditions  
450 probably of less than 10 m while the molluscan assemblage is indicative of brackish water  
451 environments. The close occurrence of this facies with F2A and F2B facies indicate nearby  
452 depositional settings. Therefore, the peloidal wackestones to packstones with calcite rafts facies  
453 reflect deposition in calm waters, supersaturated for CaCO<sub>3</sub> precipitation at the water-air  
454 interface (calcite rafts), with intermittent moderate water energy in the shallow sheltered areas  
455 of the lake in the vicinity of non-calcifying macrophyte meadows.

#### 456 **F2D: Molluscan-rich ostracod wackestone**

457 This facies consists of limestones that contain sparse to loosely packed allochems including  
458 numerous ostracods and mollusc shells as well as few ooids and peloids ([Fig. 7G-H](#)). These  
459 wackestones occur in beds of several centimetres to few tens of centimetres ([Fig. 8A](#)).  
460 Ostracods are small (around 0.5 mm) and thin-shelled and their valves may be found either  
461 articulated or disarticulated. Gastropods are often leached but their complete external moulds  
462 allow easy identification ([Fig. 7G](#)). The molluscan assemblage is widely diversified, and the  
463 community comprises essentially terrestrial and freshwater to oligo-mesohaline water taxa,  
464 among them *Lymnea (Galba)*, *Planorbis*, *Tarebia*, *Viviparus* and *Polymesoda*.

465 **Interpretation:** The molluscan-rich ostracod wackestones are formed in low energy  
466 environments as suggested by the high micrite content of the facies. The matrix of these

467 wackestones consists of inhomogeneous micrite and this likely results from ostracod burrowing  
468 and bioturbation. Burrowing and bioturbation indicate intense biological activity in very well  
469 oxygenated conditions. In addition, the molluscan assemblage, reflecting various ranges of  
470 salinity mostly freshwater for *Lymnea*, *Planorbis* and *Viviparus* and oligo-mesohaline for  
471 *Polymesoda*, indicates shallow and variable salinity settings, potentially marginal pools close  
472 to emerged wetlands or a saline lake margin at the vicinity of freshwater springs. Charophyte  
473 remains are not found thus excluding the development of calcifying meadows although non  
474 calcifying subaqueous prairies could have developed. The presence of significant amount of  
475 small ooids in F2D wackestones indicates the vicinity of oolitic bodies from which the ooids  
476 are sporadically exported into the sheltered areas. Moreover, these molluscan-rich ostracod  
477 wackestones are sharply overlain by high energy oolitic deposits (F1A) and this suggests lateral  
478 migration of the oolitic sand bodies. Finally, F2D facies is interpreted to form in low energy  
479 and shallow freshwater to brackish pools and sheltered areas of the lake margin.

### 480 **F3: Planar-laminated bindstones (microbial laminites)**

481 Microbial laminites are made of an alternation of subhorizontal to wavy and crinkled dark  
482 clotted and peloidal micrite laminae (100 microns to 1 mm thick) and light thin laminae (0.5 to  
483 1 mm) constituted of the accumulation of crushed charophyte stems and cortical cells with fine  
484 calcite spar cement (Fig. 8B-C). This facies exhibits a bindstone fabric (*sensu* Embry and  
485 Klovan, 1971) and is formed by micrite stabilization and binding of various skeletal grains  
486 including gastropod and ostracod shells as well as characean gyrogonites (Fig. 8B-C). The  
487 molluscan assemblage is dominated by the gastropod *Melanopsis acrolepta* the shells of which  
488 are entirely dissolved (Fig. 8B). The laminated bindstones show very little fenestral porosity  
489 and the presence of small-scale undulations and corrugations in the laminae may point to a  
490 microbial origin of the micrite. This facies occurs in centimetre tight beds and may form up to  
491 metre intervals of laminated limestones (Fig. 8A).

492 **Interpretation:** Planar laminated stromatolites from Tertiary basins of SE France are  
493 interpreted to form in very shallow water lacustrine environments that may experience  
494 occasional short-term emersions (e.g. [Wattine et al., 2003](#); [Lettéron et al., 2017](#)). The shallow-  
495 water conditions prevailing for the deposition of facies F3 are supported by the abundance of  
496 characean gyrogonites and stems, and by the bathymetric range of the bound molluscs  
497 (*Melanopsis*). The presence of charophyte gyrogonites indicates colonization of the lake  
498 substrate by charophyte algae in the nearby areas and suggests freshwater to slightly brackish  
499 water conditions. While stromatolites are euryhaline and tolerate a wide range of salinities (e.g.  
500 [Talbot and Allen, 1996](#)), the biological content points to freshwater to oligohaline conditions.  
501 Extant *Melanopsis* are found to live in coastal streams and freshwater to oligohaline lake waters  
502 under Mediterranean and semi-arid climates ([Plaziat and Younis, 2005](#); [Velasco et al., 2006](#);  
503 [Van Damme, 2014](#)). In the Priabonian lacustrine deposits from the Issirac basin (SE France),  
504 planar stromatolites are interpreted to form in the shallowest parts of the lake margin while the  
505 charophytes are considered to thrive at depths comprised between 0.5 m and 10 m ([Lettéron et](#)  
506 [al., 2017](#)). However, it has been documented that the development of either photosynthetic (e.g.  
507 charophytes) or microbial communities is presumably driven by changes in trophic conditions  
508 regardless of the depositional depth ([Lettéron, 2018](#)). The microbial communities can adapt to  
509 trophic changes (oligotrophic conditions) as evidence by the trapping of characean gyrogonites  
510 by the microbial binding organisms, the charophyte meadows likely occupying the deeper areas  
511 of the lake. Finally, facies F3 is interpreted to form in very shallow lake conditions under  
512 freshwater to oligo-mesohaline conditions within perennial lake body.

#### 513 **F4. Carbonate breccia with pseudomorphs after gypsum**

514 The facies F4 is found only in one bed (0.50 m) from the butte Iouton succession ([Fig. 8A](#)). It  
515 consists of a carbonate breccia displaying vertical changes in texture and diagenetic features.  
516 The lower part of the bed is made of a fractured, tight oosparite whose ooids appear to be

517 floating within sparry calcite pseudomorphs after gypsum (Fig. 8F-G). The mechanical contact  
518 between ooids argue for subsequent displacement of the grains in the initial grainstone sediment  
519 during the formation and growth of gypsum crystals. The upper part of the breccia interval is  
520 characterized by the occurrence of 1) Root traces and curved cracks (Fig. 8D) occluded by  
521 microsparite and sparite cements and 2) gypsum crystals, replaced by calcitic micrite, infilling  
522 cavities (Fig. 7D-E). These tight limestones have a total thickness of around 50 cm and are  
523 irregularly bedded and capped by an uneven surface. Furthermore, these brecciated limestones  
524 are overlain by an interval of few centimetres thick of mottled vivid red clays (Fig. 8A).

525

526 **Interpretation:** the development of curved cracks and root marks affecting the initial oolitic-  
527 peloidal grainstones (F1A facies) suggests pedogenic processes during a stage of subaerial  
528 exposition (Freytet and Plaziat, 1982; Alonso-Zarza, 2003). Grain displacement during gypsum  
529 growth indicate that sulfate precipitation occurred shortly after ooid deposition, before  
530 compaction. The presence of calcite pseudomorphs after gypsum would indicate hypersaline  
531 conditions within the paleosoil and the enrichment of water in sulphate solutes. Evaporative  
532 concentration of solutes and thereby gypsum formation necessarily reflect climate aridity and  
533 negative water inflow/evaporation. The F4 succession is therefore interpreted as representing  
534 a paleosoil horizon developed during a stage of saline lake drying.

535 .

#### 536 4.4. Vertical evolution of facies

537 The Priabonian carbonate succession from the butte Iouton is approximately 30 m thick and is  
538 characterized by the dominance of oolitic and peloidal grainstone facies (F1 facies) organized  
539 in the form of massive, horizontally bedded intervals associated with fossiliferous muds (F2  
540 facies) and stromatolite levels (F3 facies) found in the form of platelets limestones (Fig. 3).

541 Four massive intervals of oolitic grainstones (F1A facies) and peloidal grainstones (F1B facies)  
542 have been identified in the sedimentary succession and have a maximum individual thickness  
543 of about 3 m. In addition, the succession records episodic high-energy sedimentation as  
544 indicated by the regular occurrence of thin gravelly lenses and coarse-sized sands (F1C facies).  
545 Such grain-supported massive intervals are interbedded within thinly-layered limestones of  
546 wackestone to packstone texture (Facies F2A, F2B, F2C and F2D) or microbial laminites  
547 (Facies F3). The alternation of wackestone-packstone and microbial laminites with massive  
548 grainstone intervals allows the definition of 5 depositional cycles, U1 to U5, despite large  
549 masked parts (Fig. 2). Within the butte Iouton quarry, the lowermost cycle U1 (3.30 m thick)  
550 overlies the lower Eocene variegated clays and silts and displays the transition from thinly  
551 layered molluscan-rich ostracod wackestones (F2D facies) to massively bedded peloidal  
552 grainstones (F1B facies) and oolitic-peloidal grainstones (F1A facies) with scarce planar cross-  
553 stratifications: the base of the massive bed is sharp and contains gravelly-sized fossil shells  
554 accumulations (Fig. 3A-3B). The oolitic interval is capped by a subaerial exposure surface as  
555 illustrated by the development of brecciated limestones (F4 facies) and overlying paleosol  
556 horizon (Fig. 8A).

557 Cycle U2 (4.50 m thick) starts with mud-supported facies (Fig. 3A-3B) dominated by  
558 freshwater to oligo-mesohaline molluscs (F2D facies) that pass upwards into oolitic  
559 grainstones deposits (F1A facies). Above the thin oolitic bed (Fig. 7A), a 50 cm thick interval  
560 of characean-rich laminated bindstones (F3 facies) is overlain by massively bedded peloidal  
561 and oolitic grainstones (F1A and F1B facies). These grainstones become coarser and gravelly  
562 toward the top and are capped by a thin interval of oncoidal-oidal grainstone (F1C).

563 In cycle U3 (6.40 m thick) sediments are dominantly mud-supported (F2 facies) and organized  
564 into centimetre to decimeter-thick tabular strata (Fig. 7C). In the lowermost 2 metres,  
565 sedimentation is dominated by molluscan-rich ostracod wackestones (F2D facies) and

566 molluscan-rich peloidal packstone (F2A facies) together with peloidal micrites with calcite rafts  
567 (F2C facies). The upper part of the cycle is dominated by the characean-rich peloidal  
568 wackestones and packstones (F2B) and molluscan-rich peloidal packstone (F1A). The top of  
569 the cycle displays incipient pedogenic modifications (root traces, circumgranular cracks).

570 The cycle U4 (6.40 m thick) shows at its base lacustrine stromatolites (F3 facies) that pass  
571 upwards into a decimetre thick oncoidal rich grainstones (F1C facies) that gives way to a  
572 massively bedded oolitic-peloidal grainstones (F1A facies). At the top, the cycle is capped by  
573 a sharp and smooth surface. The uppermost U5 cycle (10.40 m thick) begins with a molluscan-  
574 rich ostracodal wackestones containing *Viviparus soricensis* gastropods. After an observational  
575 gap of few metres, this cycle ends with a thick oolitic and peloidal grainstone interval that is  
576 truncated by an erosional surface. This unconformity separates the Priabonian limestones from  
577 the unconformably overlying transgressive marine Burdigalian limestones characterized by the  
578 coralline red algae *Lithothamnium sp* and marine bivalves *Pecten praescabriusculus* that rest  
579 on the basal conglomerates reworking Priabonian lacustrine limestones (Fig. 3C).

580

#### 581 **4.5. Carbon and oxygen stable isotopes**

582 Prior to the analysis of the geochemical data of whole-rock bulk carbon and oxygen stable  
583 isotopes and to extract the primary geochemical signal, it is necessary to take into account the  
584 diagenetic overprints undergone by the investigated samples. In Table 2, samples have been  
585 classified as a function of the diagenetic features evidenced from macroscopic, thin-section and  
586 SEM observations. Most of the analysed samples are devoid of sparry calcite cements. In  
587 addition, in grainstone intervals (F1 facies), ooids are pervasively micritized, display significant  
588 microporosity and microrhombic calcite overgrowths (Fig. 5 C-D), while aragonitic shells are  
589 converted into calcitic micrite (Fig. 6E-F). Moderate amounts of calcite microspar cements are

590 present in a few samples of F2A facies while brecciated limestones (F4 facies) have undergone  
591 pervasive pedogenesis and pervasive sparry calcite cementation or calcite pseudomorphosis  
592 after gypsum (Fig. 8 E-G).

593 In the whole carbonate succession, samples which are devoid of sparry calcite cement and  
594 pedogenetic features exhibit negative values of  $\delta^{18}\text{O}$  and  $\delta^{13}\text{C}$  values ranging from -3.99‰ to -  
595 1.33‰ PDB and from -4.79‰ to -0.43‰ PDB, respectively (Fig. 10 A-B). Brecciated  
596 limestones (F4 facies), which are characterized by pedogenic features and sparry calcite  
597 cementation, are strongly  $^{13}\text{C}$ -depleted. Grainstone samples (F1 facies) exhibit an inverted-J  
598 pattern on  $\delta^{18}\text{O}$ - $\delta^{13}\text{C}$  plots (Fig. 10 A).

599 Measurements from cycle U1 display a very narrow range of  $\delta^{13}\text{C}$  since values which oscillate  
600 between -2.54‰ and -1.40‰ PDB while  $\delta^{18}\text{O}$  values exhibit a moderately increasing trend,  
601 with values ranging from -2.87‰ to -2.02‰ PDB (Fig. 10 B). At the top of U1,  $\delta^{13}\text{C}$  is strongly  
602 negative with values down to -5.21‰ PDB. A poorly-expressed covariant trend exists between  
603  $\delta^{13}\text{C}$  and  $\delta^{18}\text{O}$  within this cycle, especially in the oolitic-peloidal grainstones which corresponds  
604 to a part of the inverted-J trend. In cycle U2,  $\delta^{18}\text{O}$  and  $\delta^{13}\text{C}$  signals have much wider ranges of  
605 values (-3.35‰ to -1.86‰ PDB and -2.29‰ to -0.76‰ PDB respectively) and grainstone  
606 samples (F1 facies) exhibit a covariant trend similar to that of U1 cycle (Fig. 10 C). In the lower  
607 part of cycle U2, stromatolites exhibit the most  $^{13}\text{C}$ -enriched and  $^{18}\text{O}$ -depleted signatures of the  
608 available database. In cycle U3,  $\delta^{18}\text{O}$  values display little variations and range between -3.66‰  
609 and -2.64‰ PDB whereas  $\delta^{13}\text{C}$  fluctuates considerably with values ranging from -2.09‰ to -  
610 0.43‰ PDB (Fig. 10 D). Within cycles U4 and U5, samples exhibit wide ranges of  $\delta^{18}\text{O}$  with  
611 values ranging from -3.99‰ to -1.33‰ PDB and  $\delta^{13}\text{C}$  ranging from -4.79‰ to -0.53‰ PDB.  
612 Stromatolites (F3) forming the lower part of the cycle display depleted  $^{18}\text{O}$  and enriched  $^{13}\text{C}$   
613 isotope signatures.

614

## 615 **5. Discussion**

### 616 **5.1 Depositional model for an oolitic saline lake margin**

617 The analysis of carbonate microfacies, preserved biota, bedding patterns and sedimentary  
618 structures of individual lithofacies as well as the vertical succession of lithofacies enable the  
619 reconstruction of depositional models (Fig. 11) for further interpreting the vertical evolution of  
620 paleoenvironments and stages of transgression and regression of the paleolake.

621

#### 622 *Oolitic cycles (U1, U2, U4 and U5)*

623 The lower intervals of the oolitic-peloidal cycles U1, U2, U4 and U5 are made of molluscan-  
624 rich ostracod wackestones (F2D) and laminated bindstones (F3). As suggested by microfacies  
625 analysis and preserved biota, such a facies association is indicative of a deposition in a very  
626 shallow, sub-emergent, low-energy, freshwater to oligo-mesohaline lake margin. The  
627 occurrence of scattered but well preserved ooids within the molluscan-ostracodal wackestones  
628 suggests that oolitic sediments formed coevally with the F2D-F3 low-energy lake margin  
629 association. In cycles U1, U2, U4 and U5, microbial laminites or molluscan-ostracodal  
630 wackestones are sharply overlain by oolitic-peloidal (F1A) or peloidal grainstones (F1B). The  
631 high degree of sorting in oolitic-peloidal grainstone, the lack of mud matrix and the occurrence  
632 of planar cross laminations suggest an increase in water energy compared with the underlying  
633 F2D and F3 facies. The planar cross-bedded oolitic grainstones (F1A) were likely deposited at  
634 the outer part of a lacustrine margin, in the vicinity of the main oolitic factory as supported by  
635 the dominant proportion of ooids. Indeed, the significant proportion of peloids as well as the  
636 variable degree of micritization of ooids suggest that the oolitic fraction of F1A is not produced  
637 in situ but likely derives from neighbouring, high-energy, oolitic shoals. Structureless oolitic-  
638 peloidal and peloidal grainstones (F1A-F1B) likely represent a slightly calmer area, possibly in  
639 back-shoal position. The structureless nature of such carbonate sand blankets has been

640 interpreted, in shallow marine environments, as resulting from significant bioturbation of a  
641 stable substrate in a low to moderate energy back-shoal environments (Pomar et al., 2015).  
642 Additionally, peloidal grainstones exhibit significant proportions of peloidal aggregates which  
643 are interpreted to form, in modern marine environments, in area with some water circulation  
644 allowing the winnowing of fines, followed by periods of stabilization (Wanless, 1981). Finally,  
645 the vertical facies transition recorded in cycles U1, U2, U4 and U5 suggests a lake transgression  
646 and a lacustrine carbonate ramp model (Fig. 11) displaying the following facies transition from  
647 proximal to distal areas: : 1) a shallow marginal saline lake domain with deposition of planar  
648 microbial laminites (F3), and molluscan-ostracodal wackestone (F2D), 2) a more distal and  
649 open lacustrine environments with low to moderate energy characterized by the deposition of  
650 peloidal grainstones (F1B) and 3) a domain of higher energy with accumulation of ooids mixed  
651 with peloids (F1A). The area of ooid production as well as more distal (profundal) components  
652 of this lacustrine depositional model have not been captured by the studied outcrops.

653 Carbonate ramp models with oolite sand body development in open, shallow lacustrine setting  
654 have been documented in modern and ancient lacustrine environments. In the modern Great  
655 Salt Lake, similarly to the Butte Iouton lake margin, muddy sediments occupy the coastal area  
656 of the lake while oolite sand bodies develop in more open lake setting (Eardley, 1938, Bouton  
657 et al., 2019). In the Eocene Green River Formation (Utah), shoreline and protected nearshore  
658 carbonate sedimentation is characterized by mud-supported sediments with ostracods, mollusks  
659 and ooids, while shallow open lake margin is occupied by oolitic shoals (Williamson and  
660 Picard, 1974; Tänavsuu-Milkeviciene et al., 2017). In the Upper Cretaceous to Paleocene  
661 Yacoraite Formation (Argentina), a high gradient carbonate ramp model is proposed with  
662 ostracod-rich low energy eulittoral deposits protected by oolitic shoals (Deschamps et al.,  
663 2020). In the modern Lake Tanganyika, oolitic sand shoals dominate the open nearshore

664 environment while inner and more protected area are characterized by charophyte-rich  
665 calcareous silts (Cohen and Thouin, 1987).

666 The Butte Iouton lake margin shows major differences with other published depositional  
667 models involving oolite formation. In the Pliocene Glenns Ferry Oolite (Swirydczuk et al.,  
668 1980), oolite sediments occupy both foreshore and shoreface environments and no mud-rich,  
669 low energy, carbonate deposits are documented from this lake margin. In the late Triassic  
670 Clevedon lake, shoreline deposits are dominated by oolitic beachrocks while trough cross-  
671 stratified oolitic grainstones characterize shoreface sedimentation (Milroy and Wright, 2002).

672

### 673 *Mud-dominated cycle (U3)*

674 Cycle U3 exhibits a distinct facies association since ooids are relatively uncommon and  
675 sediments have dominantly muddy textures. The lower part of the cycle is characterized by an  
676 alternation of molluscan-rich peloidal packstones (F2A), peloidal wackestones to packstones  
677 with calcitic rafts (F2C) and molluscan-rich ostracod wackestones (F2D).

678 Similarly to cycles U1, U2, U4 and U5, the occurrence of F2D wackestones is indicative of  
679 very shallow, low energy environments, in the most proximal area of the lake margin. The upper  
680 part of the cycle is dominated by F2B characean wackestone which likely represents a slightly  
681 deeper (<10 m), low-energy marginal lake environment.

682 Finally, the facies succession in cycle U3 suggests a shallow, protected, low energy lake margin  
683 with extensive development of macrophytes (including charophytes and non-calcifying taxa).

684 The scarce occurrence of ooids within F2D facies suggests the coeval formation of oolitic  
685 sediment in more open area of the lake margin. However, the lack of oolitic grainstones indicate  
686 that the supersaturation with regards to carbonate minerals required for ooid formation and high

687 energy conditions have been never reached at the outcrop location during the deposition of U3  
688 cycle.

689

## 690 **5.2 Stable isotope signatures and paleohydrological implications**

691 As evidenced by [Hasiuk et al. \(2016\)](#) and as supported by petrographic evidences  
692 (microporosity and microrhombic calcite overgrowths within micritized ooids: [Fig. 5C-D](#)), the  
693 inverted-J pattern on  $\delta^{18}\text{O}$ - $\delta^{13}\text{C}$  plots ([Fig. 10A](#)) evidenced for grainstones from the whole  
694 section, likely results from neomorphic processes leading to microporosity development in  
695 meteoric environments. According to such an interpretation the  $\delta^{18}\text{O}$ - and  $\delta^{13}\text{C}$ -enriched end-  
696 member would represent the less-altered samples and therefore would approximate the primary  
697 signature of carbonate grains (ooids and peloids), the ooidal and peloidal grainstone being  
698 devoid of carbonate cement. Furthermore, the end-member of least meteoric alteration for  
699 grainstone samples (F1) ranges from -2.5‰ to 1.0‰ PDB in  $\delta^{18}\text{O}$  and from -2.0‰ and -0.5‰  
700 PDB in  $\delta^{13}\text{C}$ , which matches with primary signatures measured in late Priabonian ooid-bearing  
701 unit (Unit 2 in [Letteron et al., 2017](#)) from the Issirac basin ([Fig. 10 A](#)). Carbon and oxygen  
702 isotope signatures for wackestone-packstones (F2) and microbial laminites (F3) are  
703 significantly  $^{18}\text{O}$ -depleted compared to the end-member of least meteoric alteration for  
704 grainstones (F1). The  $^{18}\text{O}$ -depletion of stromatolites likely results from significant freshwater  
705 inputs while the  $^{18}\text{O}$ -enriched values measured in F1 grainstones may reflect either more  
706 evaporative conditions, either mixture with neighbouring saline lake water as suggested by  
707 primary isotope signatures from the Issirac basin ([Fig. 10 A](#)). The position of the Priabonian  
708 marine box ([Fig. 10 A](#), after [Veizer et al., 1999](#)) makes also possible a mixture with marine-  
709 influenced waters. Additionally, the relative  $^{13}\text{C}$ -enrichment could be partly related to a  
710 photosynthetic control on the carbon budget of the lake during the deposition of microbial  
711 (cyanobacterial) carbonates ([Talbot and Kelts, 1990](#); [Andrews et al., 1993](#); [1997](#)), as

712 particularly evidenced in microbial laminites (F3) from cycles U2, U3, U4 and U5 (Fig. 10 C-  
713 D-E) and by the vertical trend in the  $\delta^{13}\text{C}$ - $\delta^{18}\text{O}$  plot from U3.

714 In cycle U1, a poorly-expressed covariant trend exists between  $\delta^{13}\text{C}$  and  $\delta^{18}\text{O}$  (Fig. 10B),  
715 especially in the oolitic-peloidal grainstones which coincides with a segment of the overall  
716 inverted-J trend. Even though such an isotope trend likely largely result from neomorphic  
717 processes affecting micrite in meteoric environments (Léonide et al., 2014; Hasiuk et al., 2016)  
718 as suggested by petrographic observations, the interpretation of a partial preservation of a  
719 primary covariant trend cannot be entirely ruled out. Such primary covariant trends have been  
720 reported from a variety of modern lacustrine carbonates and are interpreted to result from  
721 hydrologic closure of the lake for long time periods and varying residence time of water and  
722 dissolve inorganic carbon (e.g. Talbot, 1990; Li and Ku, 1997).

723 The strongly negative excursion of  $\delta^{13}\text{C}$  at top of cycle U1 (Fig. 9) reflects the formation of  
724 pedogenic carbonates during a phase of subaerial exposition (e.g. Allan and Matthews, 1982).  
725 Negative  $\delta^{18}\text{O}$  and  $\delta^{13}\text{C}$  excursion at top of cycles U2 and U4 suggest that the cycle is capped  
726 by a subaerial exposure surface (Fig. 9) in spite of the lack of petrographic evidence. Finally,  
727 the negative  $\delta^{18}\text{O}$  and  $\delta^{13}\text{C}$  excursion at top of U4 (Fig. 9) suggests that the cycle is capped by  
728 an intraformational subaerial exposure surface, while the very negative values at top of U5 are  
729 likely to be related to meteoric overprint during the long-duration subaerial exposure preceding  
730 the Burdigalian transgression.

731

### 732 **5.3 Origin of transgressive-regressive cycles**

733 The vertical succession of lithofacies and associated depositional environments, together with  
734 stable isotope signatures allows the identification of transgressive-regressive cycles (Fig. 9) and  
735 the reconstruction of lake margin evolution and changes in paleohydrologic setting. In cycles

736 U1, U2, U4 and U5, the upward vertical facies change from mud-supported fabrics (F2 facies)  
737 or microbial laminites (F3 facies) from shallow and sheltered lake margin environments to  
738 oolitic and peloidal grainstones (F1A-B) deposited in moderate to high energy perennial  
739 waterbody records the lake transgression. The maximum flooding stage therefore occurs within  
740 the oolitic grainstone beds (F1A) which represents the most distal facies identified in the  
741 section. Pedogenetic features as well as carbon isotope signatures (Fig. 9) strongly suggest a  
742 subaerial exposition on top of these cycles which reflects the stage of maximum regression of  
743 the lake.

744 In the upper part of cycle U1, the abrupt upward vertical change in facies from oolitic-peloidal  
745 grainstone F1A to pedogenetized carbonate breccia (F4) together with the occurrence of  
746 pseudomorphs after gypsum are indicative of a forced lacustrine regression related to drying of  
747 the lake. In other oolitic cycles (U2, U4 and U5), the forced regressive stage is recorded by the  
748 subaerial exposure surfaces which sharply truncate the massive oolitic/peloidal grainstone  
749 intervals. It seems plausible to consider significant erosion during the forced regressive phase  
750 or during the early transgressive phase, as suggested by the lack of marginal/palustrine deposits  
751 preserved on top of these cycles. Moreover, it is not excluded that part of grainstone intervals  
752 has formed during a stage of normal regression. As an apparent paradox, the stable isotope  
753 signatures are indicative of greater freshwater inputs with the wackestone (F2) and microbialitic  
754 (F3) beds (lower transgressive hemicycle) than in grainstone intervals (upper transgression to  
755 normal regression?) where they suggest either a more negative inflow-evaporation balance, or  
756 a mixture with a closed lake water body or even seawater. Similarly, the vertical changes in  
757 molluscan assemblages do not indicate a salinity decrease during transgression, but on the  
758 contrary the few freshwater taxa identified (e.g. *Viviparus*, *Lymnaea*, *Planorbis*) are mainly  
759 present in the wackestone and microbialitic facies from the lower transgressive hemicycles (Fig.  
760 2). In contrast to other lake basins (e.g. Holocene, Dead Sea: [Klinger et al., 2003](#); Plio-

761 Pleistocene, Lake Turkana: [Nutz et al., 2020](#)), lake transgression does not result from an excess  
762 balance between freshwater inflow and evaporation. A lack of unequivocal control of  
763 paleohydrologic balance on transgressive/regressive cycle development has been regionally  
764 evidenced in coeval lake margin carbonate deposits from the Issirac and Saint-Chaptes basins  
765 ([Letteron et al., 2017, 2018, 2022](#)), but also in other syn-tectonic lake basins ([Chen and Hu,](#)  
766 [2017](#)).

767 Such a paradox can be explained by an increasing connexion of the Butte Iouton lake waters  
768 with regional salt waterbodies during transgression. This interpretation therefore implies that  
769 the lake basin to which the Butte Iouton carbonate margin represented an outflow of  
770 neighbouring salt water bodies. The volume of connected lake waters is controlled by a regional  
771 inflow-evaporation balance which is strongly dependent on climate conditions. In the case of  
772 Priabonian lakes from south-east France, lake closure and saline waters are associated with  
773 semi-arid conditions prevailing at regional scale ([Letteron et al., 2017, 2018](#)). In contrast, the  
774 dominantly transgressive pattern of cycles evidenced in Butte Iouton margin likely results from  
775 both 1) local subsidence driven by normal faults in a regional extensional tectonic setting which  
776 is known regionally to have started as early as the middle Priabonian ([Cavelier et al., 1984;](#)  
777 [Sanchis and Seranne, 2000](#)) and 2) saline water outflow from neighbouring regional  
778 waterbodies. Forced regression stages recorded at top of depositional cycles may result from:  
779 1) periods of increased aridity associated with a fast and significant reduction in connected lake  
780 volume, or 2) the formation of an outlet which led to the fast emptying of the lake basin ([Garcia-](#)  
781 [Castellanos, 2006](#)).

782 In Cycle U3, the upward vertical transition from the F2C and F2D wackestone/packestone  
783 indicative of very sheltered and shallow area of the lake margin to characean wackestones (F2B)  
784 suggests a transgressive trend. Similarly to oolitic cycles, molluscan assemblages and isotope  
785 signatures are indicative of a connexion with a salt waterbody (evaporative or seawater-

786 influenced lake), while the  $^{13}\text{C}$ -enrichment is likely to be related to the effect of enhanced  
787 photosynthetic activity (e.g. [Coletta et al., 2001](#); [Leng and Marshall, 2004](#)), which is consistent  
788 with the extensive development of charophytes, cyanobacteria and possibly non-calcifying  
789 macrophytes. A subaerial exposition on top of cycle U4 is evidenced from the occurrence of  
790 pedogenic features (root-traces).

791

#### 792 **5.4. The Butte Iouton outcrop: a preserved relict of a regional-scale saline lake?**

793 The vertical evolution of depositional environments and lake salinity recorded at Butte Iouton  
794 outcrop provide significant insights into the paleogeography of Priabonian paleolakes at a larger  
795 regional scale. The lack of decreasing salinity trends within the carbonate cycles, as evidenced  
796 from the persistence of oligo-mesohaline mollusks, as well as the carbon and oxygen isotope  
797 signatures strongly suggest that the transgressive trends recorded by the vertical facies evolution  
798 at Butte Iouton is not related to an increase in lake water volume resulting from an increasing  
799 inflow-evaporation balance. The present data rather support the interpretation of a carbonate  
800 sedimentation in a subsident lake basin which is fed by the outflow of adjacent saline lakes.  
801 The relatively dry conditions evidenced regionally by Priabonian lacustrine sedimentation  
802 ([Lettéron et al., 2017](#); [2018](#); [2022](#)) suggest that salinity may derive, at least partly, from a  
803 negative inflow-evaporation balance, but a salinization by recycling evaporites in the drainage  
804 area of the lake or within the lake itself is a possible interpretation. Indeed, as evidenced by  
805 [Emre and Truc \(1978\)](#), the erosion of the piercing Suzette diapir and subsequent sulfate  
806 recycling occurred coevally with the late Priabonian carbonate and evaporite sedimentation of  
807 the Mormoiron basin (~50 km north of Butte Iouton: [Fig. 12](#)). Additionally, connections with  
808 the Alpine Sea through topographic corridors may represent a possible origin for salinity in  
809 regional Priabonian lakes ([Sissingh, 2001](#)) even though a continental origin for evaporites from

810 the Valence basin has been inferred from stable isotope and mineralogical analyses (Fontes, et  
811 al., 1996).

812 The Butte Iouton outcrop is located within a 20 km-wide corridor bounded by the Nîmes fault  
813 to the NW and structured by set of SW-NE-trending normal faults (Fig. 1A). To the southeast  
814 a thick (>4000m) lacustrine sedimentation occurred in the Vistrenque Basin (Valette and  
815 Benedicto, 1995; Benedicto et al., 1996). Although the age of the lowermost syn-rift interval  
816 (Série Grise Formation: ~2000 m-thick) is unknown, the similarity in depositional polarity  
817 (siliciclastic-dominated the south and carbonate-dominated the north) between the Série Grise  
818 Formation and the Célas formation from the Sommières, Saint-Chaptes and Alès basins may  
819 suggest a Priabonian age for the lower part of the syn-rift sedimentation in the Vistrenque basin,  
820 as suggested by Cavalier et al., (1984). According to this hypothesis, the Butte Iouton outcrop  
821 would represent the northern shallow carbonate margin of a lake basin fed in siliciclastics from  
822 the southern collapsing Pyrenean reliefs. Additionally, the strike-slip movement of the Nîmes  
823 fault during a transitional tectonic phase comprised between the Pyrenean compression and the  
824 Gulf of Lion rifting (Séranne et al., 2021) is consistent with the formation of a subsiding strike-  
825 slip basin, east of the Nîmes fault, capable to accumulate a thick sedimentary cover as early as  
826 the Priabonian times. The Série Grise Formation from the Vistrenque Basin is dominantly made  
827 of organic-rich shales interbedded with thin sandstone and conglomerate horizons (Cavalier et  
828 al., 1984; Valette and Benedicto, 1995) suggesting profundal lake environments with  
829 terrigenous supplies.

830 On the footwall of the Nîmes fault, a small-sized and isolated lacustrine limestone outcrop was  
831 documented by Caziot (1896) at Puech d'Autel, within the city of Nîmes. These limestones  
832 contain a molluscan association including *Melanoïdes juliani*, *Brotia albigensis*, *Melanopsis*  
833 *acrolepta*, *Neritina*, *Galba longiscata* which is highly similar to that of the oligohaline, late  
834 Priabonian lacustrine limestones from the Issirac basin (Lettéron et al., 2017) and the Butte

835 Iouton. As a consequence, the Puech d'Autel limestones likely represent a relict outcrop of the  
836 northwestern shallow carbonate margin of the Vistrenque lake basin.

837 The proximity of the Priabonian outcrops from the Sommières and Saint-Chaptes basins (10  
838 km) makes a connection with the ASCI saline lake strongly possible. Additionally, in the Issirac  
839 basin, [Lettéron et al. \(2017\)](#) argued for a correlation between maximum lacustrine  
840 transgressions and periods with the most deficient inflow-evaporation balance. These authors  
841 interpreted this apparent paradox as resulting from a connection of the Issirac lake waters with  
842 those of the Mormoiron and Vistrenque basins, during a period of relative aridity.

843 The presence of isolated outcrops of Priabonian lacustrine limestones with brackish fauna, 10  
844 km northeast of the eastern termination of the Saint-Chaptes basin, near Uzès ([BRGM, 1968](#))  
845 ([Fig. 12](#)), shows that the ASCI lake basin had a significantly wider extension towards the east  
846 and that a connection with the Vistrenque basin is a plausible hypothesis. As a consequence,  
847 various potential sills which could have connected the ASCI lake system with the Vistrenque-  
848 Mormoiron may be identified west of the Nîmes fault. More broadly, the dominant  
849 transgressive character of depositional sequences recorded locally in various Priabonian  
850 carbonate lake margins from southeast France (Issirac: [Lettéron et al., 2017](#); Saint-Chaptes:  
851 [Lettéron et al., 2018](#); Alès: [Lettéron et al., 2022](#); Butte Iouton: this study) associated with a  
852 persistence of oligo-mesohaline waters in a context of negative inflow-evaporation balance is  
853 indicative of interconnected, subsiding lacustrine area, the total volume of connected waters  
854 being much larger than that of individual lake basin ([Fig. 12](#)).

855 Finally, the oolitic carbonate ramp developing on the margins of the Vistrenque lake margin  
856 show significant analogies with various marine oolitic ramps regarding the overall facies model  
857 (e.g. Mississippian from Wales: [Burchette et al., 1990](#); Upper Jurassic from Spain: [Pomar et al.,](#)  
858 [2015](#); Jurassic from Morocco: [Shekhar et al., 2014](#)): 1) oolite shoal developing on the outer  
859 ramp, 2) poorly structured oolitic grainstones forming in backshoal setting, 3) mud-supported

860 and/or microbial carbonates developing in the low-energy, innermost area of the ramp and 4)

861 the ramp distally passes into deep water environments.

862

## 863 6. Conclusion

864

865 The integrative approach (biostratigraphy, paleoecology, carbonate petrography, sedimentology  
866 and stable isotope geochemistry) applied to the study of lacustrine carbonates from Butte Iouton  
867 outcrops allowed reconstructing a depositional model for an oolitic saline lake margin and  
868 providing new insights into the Priabonian paleogeography of southeast France.

869 1) An oolitic lacustrine ramp model has been evidenced and displays the following facies  
870 transition from proximal to distal areas: 1) a shallow marginal saline lake domain with  
871 deposition of planar microbial laminites, and molluscan-ostracodal wackestone, 2) a more  
872 distal and open lacustrine environments with low to moderate energy characterized by the  
873 deposition of peloidal grainstones and 3) a domain of higher energy with accumulation of  
874 ooids mixed with peloids. The area of ooid production (not captured by the studied outcrops)  
875 likely consisted in oolitic shoals within a high energy outer ramp setting.

876 2) Carbonate sedimentation dominantly occurred during stages of lake transgression. Subaerial  
877 exposure surfaces evidenced at top of depositional cycles are interpreted to result from forced  
878 regressions which occurred during periods of negative inflow-evaporation balance.

879 3) Molluscan associations suggest that oligo- to mesohaline waters dominantly prevailed during  
880 the studied time interval.

881 4) The apparent paradox between a dominant transgressive sedimentation and the persistence  
882 of saline conditions suggest that lake transgression is controlled by subsidence and outflows  
883 from neighbouring saline waterbodies, and not by an increase in regional lake water volume.  
884 The studied carbonate margin belongs to a set of interconnected saline lake waterbodies  
885 whose total volume is much greater than that created locally by subsidence.

886 5) The compilation of existing data regarding regional Priabonian deposits supports the  
887 interpretation of interconnected saline lake basins characterized by a siliciclastic-dominated  
888 southern margin whose sediment is sourced from the collapsing Pyrenean reliefs and by a

889 carbonate-dominated northern margin with significant oolitic sedimentation in high-energy  
890 nearshore area.

891

## 892 **References**

893 Allan JR, Matthews, R. 1982. Isotope signatures associated with early meteoric diagenesis.  
894 *Sedimentology* 29 (6): 797-817.

895 Alonso-Zarza AM. 2003. Palaeoenvironmental significance of palustrine carbonates and  
896 calcretes in the geological record. *Earth-Science Reviews* 60: 261–298.

897 Andrews JE, Riding R, Dennis PF. 1993. Stable isotopic composition of recent freshwater  
898 cyanobacterial carbonates from the British Isles: local and regional environmental controls.  
899 *Sedimentology* 40: 303–314.

900 Andrews JE, Riding R, Dennis PF. 1997. The stable isotopic record of environmental and  
901 climatic signals in modern terrestrial microbial carbonates from Europe. *Palaeogeogr*  
902 *Palaeoclimatol Palaeoecol* 129: 171–189.

903 Arenas C, Cabrera L, Ramos E. 2007. Sedimentology of tufa facies and continental  
904 microbialites from the Paleogene of Mallorca Island (Spain). *Sedimentary Geology* 197: 1-27.

905 Arthaud F, Ogier M, Séguret M. 1981. Géologie et géophysique du Golfe du Lion et de sa  
906 bordure nord. *Bulletin du BRGM* 1(3): 175–193.

907 Benedicto A, Labaume P, Séguret M, Séranne M. 1996. Low-angle crustal ramp and basin  
908 geometry in the Gulf of Lion passive margin: the Oligocene-Aquitania Vistrenque graben, SE  
909 France. *Tectonics* 15(6): 1192–1212.

910 BRGM. 1968. Notice de la carte géologique de la France au 1/50000: feuille Uzès n°939 : 12  
911 pp.

912 Bodergat A-M, Briot D, Huguency M, Poidevin J-L, Picot L, Giraud F, Berger J.P, Levy A,  
913 Poignant A. 1999. Incursions marines dans l'environnement lacustre du rift oligocène de  
914 Limagne (Massif Central, France) : apport des organismes halophiles et des isotopes du  
915 strontium, datation par les mammifères. *Bulletin de la Société Géologique de France* 170: 499–  
916 511.

917 Bouton A, Vennin E, Amiotte-Suchet P, Thomazo C, Sizun, J-P, Virgone A, Gaucher EC,  
918 Visscher PT. 2019. Prediction of the calcium carbonate budget in a sedimentary basin: A  
919 “source-to-sink” approach applied to Great Salt Lake, Utah, USA. *Basin Research* 32, 1005-  
920 1034.

921 Briot D, Poidevin JL. 1998. Stratigraphie  $^{87}\text{Sr}/^{86}\text{Sr}$  de quelques laminites carbonates du  
922 Rupélien inférieur du fossé de Limagne: incursions marines dans le rift du Massif central  
923 français?. *Compte Rendus de l'Académie des Sciences, Paris* 236: 479–483.

924 Burchette TP, Wright VP, Faulkner TJ. 1990. Oolitic sandbody depositional models and  
925 geometries, Mississippian of southwest Britain: implications for petroleum exploration in  
926 carbonate ramp settings. *Sedimentary Geology* 68: 87-115.

927 Cavelier C, Alabouvette G, Amberger J-P, Cautru J-P, Charollais J, Chateauneuf J-J, Crochet  
928 J-Y, Campredon R, Debeglia N, Durand J-P, Feist-Castel M, Freytet P, Gannat E, Gaudant J,  
929 Giannerini G, Godinot M, Hartenberger J-L, Huguency M, Kerckhove C, Lefavrais-Raymond  
930 A, Legendre S, Lespinasse P, Magne J, Nury D, Pairis J-L, Plaziat J-C, Rémy J-A, Schlund J-  
931 M, Sige, B, Sittler C, Sudre J, Trauth N, Truc G, Valleron M-M, Vianney-Liaud M, Villatte, J.  
932 1984. Paléogène. In : Debrand-Passard ed., *Synthèse géologique du Sud-Est de la France*.  
933 *Mémoire du BRGM* 125 : pp. 389-468.

- 934 Caziot M. 1896. Sur le Tertiaire inférieur des environs de Nîmes. *Bulletin de la Société*  
935 *Géologique de France* 24: 1–32.
- 936 Chen M, Hu X. 2017. Regression-transgression cycles of paleolakes in the Fen River Graben  
937 Basin during the mid to late Quaternary and their tectonic implication. *Frontiers in Earth*  
938 *Sciences* 11(4): 703–714.
- 939 Cohen AS, Thouin C. 1987. Nearshore carbonate deposits in Lake Tanganyika. *Geology* 15:  
940 414-418.
- 941 Coletta P, Pentecost A, Spiro B. 2001. Stable isotopes in charophyte incrustations: relationships  
942 with climate and water chemistry. *Palaeogeography, Palaeoclimatology, Palaeoecology* 173:  
943 9-19.
- 944 Daley B. 1972. Macroinvertebrate assemblages from the Bembridge marls (Oligocene) of the  
945 Isle of Wight, England, and their environmental significance. *Palaeogeography,*  
946 *Palaeoclimatology, Palaeoecology* 11(1): 11–32.
- 947 Dalrymple RW. 1992. Tidal depositional systems. In: R. G. Walker and N. P. James, eds. *Facies*  
948 *Models and Sea Level Changes, Geological Association of Canada*: 195-218.
- 949 Davaud E, Girardclos S. 2001. Recent freshwater ooids and oncoids from western Lake Geneva  
950 (Switzerland): indications of a common organically mediated origin. *Journal of Sedimentary*  
951 *Research* 71(3): 423-429.
- 952 De Roys M. 1846. Note sur la comparaison des bassins tertiaires du Midi avec celui de Paris.  
953 *Bulletin de la Société Géologique de France* (2ème série) (3): 645-652.
- 954 Deschamps R, Rohais S, Hamon Y, Gasparini M. 2020. Dynamic of a lacustrine sedimentary  
955 system during late rifting at the Cretaceous–Palaeocene transition: Example of the Yacoraite  
956 Formation, Salta Basin, Argentina. *The depositional Record* 6: 490-523.

957 Dèzes P, Schmid S.M, Ziegler P.A. 2004. Evolution of the European Cenozoic Rift System:  
958 interaction of the Alpine and Pyrenean orogens with their foreland lithosphere. *Tectonophysics*  
959 389: 1–33.

960 Dromart G, Dumas D. 1997. The salt basin of Valence (France). In: Busson G, Schreiber B.C.  
961 eds., *Sedimentary Deposition in Rift and Foreland Basins in France and Spain*. Columbia Univ.  
962 Press, New York: pp. 195–239.

963 Dumas E. 1876. *Statistique Géologique, Minéralogique, Métallurgique et Paléontologiques du*  
964 *Département du Gard*. Arthus Bertrand ed. : 735 pp.

965 Dunham RJ. 1962. Classification of Carbonate Rocks According to Depositional Texture. In:  
966 Ham, W.E., Ed., *Classification of Carbonate Rocks*, AAPG, Tulsa, 108-121.

967 Eardley AJ. 1938. Sediments of Great Salt Lake, Utah. *AAPG Bulletin* 22, 1305–1411.

968 Embry AF, Klovan JE. (1971) A Late Devonian Reef Tract on Northeastern Banks Island.  
969 *Canadian Petroleum Geology*, 19, 730-781.

970 Emre T, Truc G. 1978. Mise en évidence d'un contact discordant Oligocène-Trias dans le  
971 massif de Suzette. Implications tectoniques et conséquences sur l'origine des évaporites  
972 ludiennes du bassin de Mormoiron (Vaucluse). *Géologie Alpine* 54: 17–23.

973 Esu D, Girotti O. 2010. The Late Oligocene Molluscan Fauna from Otranto (Apulia, Southern  
974 Italy): an example of alternating freshwater, lagoonal and emerged  
975 environments. *Palaeontology* 53(1): 137-174.

976 Fontannes F. 1884. Description sommaire de la faune malacologique des formations saumâtres  
977 et d'eau douce du groupe d'Aix (Bartonien – Aquitanien) dans le bas Languedoc, la Provence  
978 et le Dauphiné. Georg H, Lyon, and Savy F, Paris: 60 pp.

- 979 Fontes J-C, Filly A, Gaudant J, Durringer P. 1991. Origine continentale des évaporites  
980 paléogènes de Haute Alsace : arguments paléoécologiques, sédimentologiques et isotopiques.  
981 *Bulletin de la Société Géologique de France* 162: 725–737.
- 982 Fontes J-C, Gaudant J, Mélières F, Filly A, Schlund J-M. 1996. Origine continentale des  
983 évaporites paléogènes du fossé de Valence (Drôme): données minéralogiques, isotopiques et  
984 paléoécologiques. *Bulletin de la Société Géologique de France* 167(4): 475–481.
- 985 Fretter V, Graham A. (1978). The prosobranch molluscs of Britain and Denmark. Part 3 –  
986 Neritacea, Viviparacea, Valvatacea, terrestrial and freshwater Littorinacea and  
987 Rissoacea. *Journal of Molluscan Studies*. Suppl. 5: 1-152.
- 988 Freytet P, Plaziat J-C. 1982. Continental carbonate sedimentation and pedogenesis – Late  
989 Cretaceous and Early Tertiary of Southern France. In: Purser B. H. ed., *Contribution to*  
990 *Sedimentology*, Schweizerbart'sche Verlag, Stuttgart, 12: 217 pp.
- 991 Gallois A, Bosence D, Burgess PM. 2018. Brackish to hypersaline facies in lacustrine  
992 carbonates: Purbeck Limestone Group, Upper Jurassic–Lower Cretaceous, Wessex Basin,  
993 Dorset, UK. *Facies* 64, 12.
- 994 Garcia A. 1994. Charophyta: their use in paleolimnology. *Journal of Paleolimnology* 10(1):  
995 43–52.
- 996 Garcia A, Chivas A.R. 2006. Diversity and ecology of extant and Quaternary Australian  
997 charophytes (Charales). *Cryptogamie Algologie* 27(4): 323–340.
- 998 Garcia-Castellanos D. 2006. Long-term evolution of tectonic lakes: Climatic controls on the  
999 development of internally drained basins. *Geological Society of America Special Paper* 398:  
1000 283-294.

- 1001 Gorini C, Le Marrec A, Mauffret A. 1993. Contribution to the structural and sedimentary  
1002 history of the Gulf of Lions (western Mediterranean), from the ECORS profiles, industrial  
1003 seismic profiles and well data. *Bulletin de la Société géologique de France* 164(3): 353–363.
- 1004 Grambast L, Grambast-Fessard N. 1981. Étude sur les Charophytes tertiaires d'Europe  
1005 occidentale III: le Genre Gyrogonia. *Paléobiologie Continentale* 12(2): 1-35.
- 1006 Hargrave JE, Hicks MK, Scholz CA. 2014. Lacustrine carbonates from Lake Turkana, Kenya:  
1007 a depositional model of carbonates in an extensional basin. *Journal of Sedimentary Research*  
1008 84: 224-237.
- 1009 Harris M, Faulkner P, Asmussen B. 2015. Macroscopic approaches to the identification of  
1010 expedient bivalve tools: a case study investigating polymesoda (=Geloina) coaxans (Bivalvia:  
1011 Corbiculidae) shell valves from Princess Charlotte Bay, Queensland, Australia. *Quaternary*  
1012 *International* 427: 201–215.
- 1013 Hasiuk FJ, Kaczmarek SE, Fullmer SM. 2016. Diagenetic origins of the calcite microcrystals  
1014 that host microposity in limestone reservoirs. *Journal of Sedimentary Research*, 86, 1163-1178.
- 1015 Kahle CF. 1974. Ooids from Great Salt Lake, Utah, as analogue for the genesis and diagenesis  
1016 of ooids in marine limestones. *Journal of Sedimentary Geology* 44(1): 30-39.
- 1017 Klinger Y, Avouac J-P, Bourlès D, Tisnérat N. 2003. Alluvial deposition and lake-level  
1018 fluctuations forced by Late Quaternary climate change: the Dead Sea case example.  
1019 *Sedimentary Geology*: 162 (1-2): 119-139.
- 1020 Leng MJ, Marshall JD. 2004. Palaeoclimate interpretation of stable isotope data from lake  
1021 sediment archives. *Quaternary Science Reviews* 23(7-8): 811-831.
- 1022 Léonide P, Fournier, F, Reijmer JJG, Vonhof H, Borgomano J, Dijk J, Rosenthal M, van  
1023 Goethem M, Cochard J, Meulenaars K. 2014. Diagenetic patterns and pore space distribution

1024 along a platform to outer-shelf transect (Urgonian limestone, Barremian-Aptian, SE France).  
1025 *Sedimentary Geology*: 306, 1-28.

1026 Lesueur J-L. 1991. Etude sédimentologique et stratigraphique du Bassin Paléogène d’Apt–  
1027 Manosque–Forcalquier (Alpes de Haute Provence). Modalités de la transition Burdigalienne.  
1028 Ph.D. thesis, University M. de Montaigne, Bordeaux III, France : 407 pp.

1029 Lettéron A. 2018. Caractérisation sédimentologique, stratigraphique et paléoenvironnementale  
1030 du système carbonaté lacustre à salinité variable du bassin d’Alès et des régions limitrophes  
1031 (Priabonien, SE France) : implications paléoclimatiques et paléogéographiques. PhD thesis,  
1032 Aix-Marseille University : 344 pp.

1033 Lettéron A, Fournier F, Hamon Y, Villier L, Margerel J-P, Bouche A, Feist M, Joseph P. 2017.  
1034 Multi-proxy paleoenvironmental reconstruction of saline lake carbonates: Paleoclimatic and  
1035 paleogeographic implications (Priabonian-Rupelian, Issirac Basin, SE France). *Sedimentary*  
1036 *Geology* 358 : 97–120.

1037 Lettéron A, Hamon Y, Fournier F, Séranne M, Pellenard P, Joseph P. 2018. Reconstruction of  
1038 a saline, lacustrine carbonate system (Priabonian, St-Chaptes Basin, SE France): depositional  
1039 models, paleogeographic and paleoclimatic implications. *Sedimentary Geology* 367: 20–47.

1040 Lettéron A, Hamoun Y, Fournier F, Demory F, Séranne M, Joseph P. 2022. Stratigraphic  
1041 architecture of a saline lake system: From lake depocenter (Alès Basin) to margins (Saint-  
1042 Chaptes and Issirac basins), Eocene-Oligocene transition, south-east France. *Sedimentology*,  
1043 *Blackwell Publishing, in press*, <DOI: 10.1111/sed.12920>, <hal-03406458>.

1044 Li H-C, Ku .-L. 1997.  $\delta^{13}\text{C}$ - $\delta^{18}\text{O}$  covariance as a paleohydrological indicator for closed-basin  
1045 lakes. *Palaeogeography, Palaeoclimatology, Palaeoecology* 133: 69 80.

1046

1047 Mauffret A, Gorini C. 1996. Structural style and geodynamic evolution of Camargue and  
1048 Western Provencal basin, southeastern France. *Tectonophysics* 15(2): 356-375.

1049 Ménillet F. 1973. Carte géologique de la France au 1/50000, feuille Nîmes, BRGM Edition.

1050 Milroy PG, Wright VP. 2002. Fabrics, facies control and diagenesis of lacustrine ooids and  
1051 associated grains from the Upper Triassic, southwest England. *Geological Journal* 37: 35-53.

1052 Miranda NAF, Perissinotto R, Appleton CC. 2010. Salinity and temperature tolerance of the  
1053 invasive freshwater gastropod *Tarebia granifera*. *South African Journal of Science* 106(3/4):  
1054 Art. #156, 7 pages. DOI: 10.4102/sajs.v106i3/4.156.

1055 Morton B, 1983. Mangrove bivalves. In: Russell-Hunter, W.D. ed., *The Mollusca* 6, Academic  
1056 Press, Orlando: pp. 77–138.

1057 Nutz A, Schuster M, Barboni D, Gassier G, Van Bocxlaer B, Robin C, Ragon T, Ghienne J-F,  
1058 Rubino J-L. 2020. Plio-Pleistocene sedimentation in West Turkana (Turkana Depression,  
1059 Kenya, East African Rift System): Paleolake fluctuations, paleolandscapes and controlling  
1060 factors. *Earth Science Reviews* 111: 103415.

1061 Pellat E, Allard M. 1895. Dépôts lacustres de la Butte Iouton entre Comps et Beaucaire (Gard).  
1062 *Bulletin de la Société Géologique de France* 23: 434-436.

1063 Plaziat J-C, Younis WR. 2005. The modern environments of Molluscs in southern  
1064 Mesopotamia, Iraq: A guide to paleogeographical reconstructions of Quaternary fluvial,  
1065 palustrine and marine deposits. *Carnets de Géologie* 2005/01, (18pp).

1066 Pomar L, Aurell M, Badenas B, Morsilli M, Al-Awwad S.F. 2015. Depositional model for a  
1067 prograding oolitic wedge, Upper Jurassic, Iberian basin. *Marine and Petroleum Geology*  
1068 67: 556-582.

- 1069 Reichenbacher BA, Uhlig U, Kowalke T, Bassler B, Matzke-Karasz Schenk B. 2004. Biota,  
1070 paleoenvironments and biostratigraphy of continental Oligocene deposits of the South German  
1071 Molasse Basin (Penzberg syncline). *Palaeontology* 47(3): 639–677.
- 1072 Riveline J. 1986. Les charophytes du Paléogène et du Miocène inférieur d'Europe occidentale.  
1073 Cahiers de Paléontologie, volume 8). Muséum national d'Histoire naturelle, Paris. 304 pp.
- 1074 Riveline J, Berger J.-P, Feist M, Martin-closas C, Schudack M, Soulié-Märsche I. 1996.  
1075 European Mesozoic-Cenozoic charophyte biozonation. *Bulletin de la Société Géologique de*  
1076 *France* 167(3): 453–468.
- 1077 Roduit N. 2007. JMicroVision: un logiciel d'analyse d'images pétrographiques polyvalent. PhD  
1078 thesis, University of Geneva, 128 p.
- 1079 Roman F. 1903. Contributions à l'étude des Bassins lacustres de l'Éocène et de l'Oligocène  
1080 du Languedoc. *Bulletin de la Société Géologique de France (4<sup>ème</sup> série)* 3: 546-616.
- 1081 Roman F. 1910. Faune saumâtre du sannoisien du Gard. *Bulletin de la Société Géologique de*  
1082 *France (4<sup>ème</sup> série)* 10: 927–955.
- 1083 Rouchy J-M. 1997. Paleogene continental rift system of Western Europe: locations of basins,  
1084 paleogeographic and structural framework, and the distribution of evaporites. In: Busson, G.,  
1085 Schreiber, B.C. eds., *Sedimentary Deposition in Rift and Foreland Basins in France and Spain*.  
1086 Columbia Univ. Press, New York: pp. 45–94.
- 1087 Rouchy J-M, Blanc-Valleron M-M. 2009. Les évaporites matériaux singuliers, milieux  
1088 extrêmes. Vuibert, Paris : 184 pp.
- 1089 Sanchis E, Séranne M. 2000. Structural style and tectonic evolution of a polyphase extensional  
1090 basin of the Gulf of Lion passive margin: the Tertiary Alès Basin, southern France.  
1091 *Tectonophysics* 322: 243–264.

1092 Sandberg PA. 1975. New interpretations of Great Salt Lake ooids and of ancient non-skeletal  
1093 carbonate mineralogy. *Sedimentology* 22: 497-537.

1094 Sandberg PA. 1980. The Pliocene Glenns Ferry oolite: lake-margin carbonate deposition in the  
1095 southwestern Snake River plain—Discussion and replay. *Journal of Sedimentary Petrology* 50:  
1096 997–998.

1097 Séranne M, Benedicto A, Truffert C, Pascal G, Labaume P. 1995. Structural style and evolution  
1098 of the Gulf of Lion Oligo-Miocene rifting: Role of the Pyrenean orogeny. *Marine and*  
1099 *Petroleum Geology* 12: 809–820.

1100 Séranne M, Couëffé R, Husson E, Baral C, Villard J. 2021. The transition from Pyrenean  
1101 shortening to Gulf of Lion rifting in Languedoc (South France) –A tectonic-sedimentation  
1102 analysis. *BSGF - Earth Sciences Bulletin* 192, 27.

1103 Shekhar R, Sahni I, Benson G, Agar S, Amour F, Tomas S, Christ N, Always R, Mutti M,  
1104 Immenhauser A, Karcz Z, Kabiri L. 2014. Modelling and simulation of a Jurassic carbonate  
1105 ramp outcrop, Amellago, High Atlas Mountains, Morocco. *Petroleum Geoscience* 20, 109–124.

1106 Sissingh W. 2001. Tectonostratigraphy of the West Alpine Foreland: correlation of Tertiary  
1107 sedimentary sequences, changes in eustatic sea-level and stress regimes. *Tectonophysics*: 333,  
1108 361–400.

1109 Schäfer A, Stapf, KRG. 1978. Permian Saar-Nahe Basin and recent Lake Constance (Germany):  
1110 two environments of lacustrine algal carbonates. In: A. Matter and M.E. Tucker (Eds), *Modern*  
1111 *and Ancient Lake Sediments*. IAS Special Publication, 2, 83-107.

1112 Swirydczuk K, Wilkinson BH. 1979. The Pliocene Glenns Ferry oolite: lake-margin carbonate  
1113 deposition in the southwestern Snake River plain. *Journal of Sedimentary Petrology* 49: 995–  
1114 1004.

- 1115 Swirydczuk K, Wilkinson BH, Smith GR. 1980. The Pliocene Glenns Ferry oolite—II:  
1116 Sedimentology of oolitic lacustrine terrace deposits. *Journal of Sedimentary Petrology* 50:  
1117 1237–1248.
- 1118 Tabb DC, Moore DR. 1971. Discovery of the Carolina Clam, *Polymesoda caroliniana* (Bosc),  
1119 a supposed Florida disjunct species, in Everglades National Park, Florida. *Gulf Research*  
1120 *Reports* 3(2): 265–281.
- 1121 Talbot MR. 1990. A review of the palaeohydrological interpretation of carbon and oxygen  
1122 isotopic ratios in primary lacustrine carbonates. *Chemical Geology* 80: 261–279.
- 1123 Talbot MR, Allen PA, 1996. Lakes. In: Reading, H.G. ed., *Sedimentary Environments:*  
1124 *Processes. Facies and Stratigraphy*. Blackwell Science, Oxford: pp. 83–124.
- 1125 Tānavsū-Milkeviciene K, Sarg JF, Bartov Y. 2017. Depositional Cycles and Sequences in an  
1126 Organic-Rich Lake Basin: Eocene Green River Formation, Lake Uinta, Colorado and Utah,  
1127 U.S.A. *Journal of Sedimentary Research* 87(3): 210-229.
- 1128 Triat JM, Truc G. 1974. Evaporites paléogènes du domaine rhodanien. *Revue de Géographie*  
1129 *Physique et de Géologie Dynamique* 16: 235–262.
- 1130 Truc G. 1978. Lacustrine Sedimentation in an Evaporitic Environment: The Ludian  
1131 (Palaeogene) of the Mormoiron Basin, Southeastern France. *Special Publications of the*  
1132 *International Association of Sedimentologists* 2: 189–203.
- 1133 Valette M. 1991. Etude structural du gisement salifère Oligocène de Vauvert (Gard), *Thèse de*  
1134 *doctorat*, Univ. Montpellier II, 229 pp.
- 1135 Valette M, Benedicto A. 1995. Chevauchements gravitaires halotectoniques dans le bassin  
1136 distensif de Camargue (marge du golfe du Lion, SE de la France). *Bulletin de la Société*  
1137 *Géologique de France* 166(2): 137-147.

1138 Veizer J, Ala D, Azmy K, Bruckschen P, Buhl D, Bruhn F, Carden G, Diener A, Ebner S,  
1139 Godderis Y, Jasper T, Korte C, Pawellek F, Podlaha O, Strauss H. 1999.  $^{87}\text{Sr}/^{86}\text{Sr}$ ,  $\delta^{13}\text{C}$  and  
1140  $\delta^{18}\text{O}$  evolution of Phanerozoic seawater. *Chemical Geology* 161 (1–3): 59–88.

1141 Velasco J, Millán A, Hernández J, Hernández J, Gutiérrez C, Abellán P, Sánchez D, Ruiz M.  
1142 2006. Response of biotic communities to salinity changes in a Mediterranean hypersaline  
1143 stream. *Aquat. Biosyst.* 2, 12. <https://doi.org/10.1186/1746-1448-2-12>

1144 Van Den Berg MS, Coops H, Simons J, De Keizer A. 1998 – Competition between *Chara*  
1145 *aspera* and *Potamogeton pectinatus* as a function of temperature and light. *Aquatic botany* 60:  
1146 241-250.

1147 Wanless HR. 1981. Fining-upward sedimentary sequences generated in seagrass beds. *Journal*  
1148 *of Sedimentary Petrology* 51: 445-454.

1149

1150 Wattine A, Vennin E, De Wever P, 2003. Evolution d'un environnement carbonaté lacustre à  
1151 stromatolithes, par l'approche paleo-écologique (Carrière de Montaigu-le-Blin, bassin de  
1152 Limagne, Allier, France). *Bulletin de la Société Géologique de France* 174 (3): 243-260.

1153 Williamson CR, Picard M.D. 1974. Petrology of carbonate rocks of the Green River Formation  
1154 (Eocene). *Journal of Sedimentary Petrology* 44(3):738-759.

1155 Ziegler PA. 1992. European Cenozoic rift system. In: Ziegler, P.A. (Ed.), Geodynamics of  
1156 Rifting, Volume I, Case History Studies on Rifts: Europe and Asia. *Tectonophysics* 208: 91–  
1157 111.

1158

1159

1160

1161 **Figure captions**

1162 **Figure 1:** A) Simplified structural map of Languedoc and southern Rhône valley (SE France)  
1163 (after [Séranne et al., 2021](#); [Mauffret and Gorini, 1996](#)): the grey shaded areas indicate late  
1164 Eocene to Aquitanian deposits (after [Séranne et al., 1995](#); [Séranne et al., 2021](#)) and the  
1165 background map displays the Bouguer anomaly (after [Arthaud et al., 1980](#)). B) Geological map  
1166 of the Comps and Butte Iouton area, modified from the BRGM geological map, Nîmes sheet  
1167 1/50000 ([Ménillet, 1973](#)): the map shows the Eocene to Miocene outcrops and the Cretaceous  
1168 substratum of the Jonquières high. C) Detailed geological map displaying the close-up view of  
1169 the box around the butte Iouton hill in B).

1170 **Figure 2:** Detailed sedimentary log of the butte Iouton succession and main molluscan taxa  
1171 identified on field. Most of the section is measured on the quarry (see location in Fig. 1C). See  
1172 text for the definition of lithofacies and sedimentary cycles.

1173 **Figure 3:** Field photographs from the Butte Iouton quarry. A) Stratal succession from U1 to  
1174 U3 cycles showing the thick and horizontally layered oolitic-peloidal grainstone beds. B) Close  
1175 view on stratal succession from U1 and U2 cycles C) Erosional contact between Priabonian  
1176 lacustrine oolitic grainstones and overlying Burdigalian bioclastic limestone. Priabonian  
1177 limestone clasts are reworked within the Burdigalian deposits (black arrows).

1178 **Figure 4:** Charophyte gyrogonites and key gastropods and bivalves from the butte Iouton  
1179 limestones. A-B: SEM photographs of characean gyrogonites from the lowermost characean-  
1180 rich microbial laminites. A: *Gyrogona caelata* (Reid and Groves, 1921), lateral view. B:  
1181 *Gyrogona* aff. *lemanii capitata* (Grambast and Grambast-Fessard, 1981) lateral view. C-K:  
1182 Common molluscan taxa. C) *Lymnea Ioutensis* (Roman, 1910). D) *Planorbis stenocyclotus*  
1183 (Fontannes, 1884). E) *Brotia Albigensis* (Noulet, 1854). F) *Tarebia barjacensis* (Fontannes,  
1184 1884). G) *Melanopsis acrolepta* (Fontannes, 1884). H) *Hydrobia celasensis* (Fontannes, 1884).

1185 I) *Assimineea nicolasi* (Roman, 1910). J) *Nystia plicata* (d'Archiac & Verneuil, 1855). K)  
1186 *Polymesoda dumasi* (M. de Serres, 1827). Scale bar is 5 mm.

1187

1188 **Figure 5:** Microstructure of ooids. A) Thin-section microphotograph under polarized-light  
1189 microscopy showing the variably preserved radiaxial microstructure within the cortex and the  
1190 occurrence of micritized areas (arrows). The inner part of the ooid is pervasively micritized and  
1191 the nucleus consists of a quartz grain. B) Detail of the radiaxial microstructure of ooid cortex  
1192 under reflected-light microscopy. C) SEM photograph of a thin-sectioned micritized ooid  
1193 showing the euhedral to subhedral micrite probably replacing the initially radiaxial  
1194 microstructure and the presence of significant inter-crystalline microporosity. D) Close-up on  
1195 the outer cortex of a micritized ooid under SEM showing microrhombic calcite overgrowths  
1196 (arrow).

1197

1198 **Figure 6:** Oolitic-peloidal and peloidal grainstones facies (F1). A-B-E-F-G) Thin section  
1199 microphotographs under plane polarized light; C-D: Field photographs. A) Oolitic-peloidal  
1200 grainstone (Facies F1A) showing a mixture of ooids (white arrow) and peloids (grey arrow).  
1201 Note the bimodal distribution of grains: the medium-sized grains include superficial, radiaxial  
1202 and strongly micritized ooids while the peloids are the finer (around 0.1 – 0.2 mm size) and  
1203 structureless grains. The nuclei of the ooids are essentially made of peloids. B) Well-sorted  
1204 oolitic-peloidal grainstone displays abundant radiaxial ooids (white arrow) and few peloids  
1205 (grey arrow). The nuclei of the ooids consist of quartz grains or bioclasts. Note the high amount  
1206 of intergranular porosity and the almost lack of compaction features. C) Field photograph of  
1207 the southern face of the quarry showing a massive bed of oolitic peloidal grainstones with  
1208 decimetre-thick, gravelly fossiliferous lenses. Cross-stratifications are seldom visible (see Fig.

1209 6D). D) Close-up view of sub-planar cross-stratification from the oolitic-peloidal grainstones  
1210 indicated by the dotted lines. The cross-beddings heights range between 10 and 50 cm. E)  
1211 Peloidal grainstones with scattered molluscs (F1B facies) displaying slightly elongated peloids,  
1212 micritized molluscan shells (mainly gastropods: *Gast.*) and few aggregate grains (*Agg.*). F)  
1213 Oncoidal-oidal rich peloidal grainstones (F1C facies) are poorly sorted sands consisting of a  
1214 mixture of peloids and coarse grains (coated grains and molluscs). Note the strong  
1215 micritization of the molluscan shells (*Moll.*). G) F1C facies displays bimodal distribution made  
1216 of millimetric coated grains (oids and/or oncoids) floating in a peloidal sand matrix: F1C facies  
1217 occurs generally within few centimetres thick lenses.

1218

1219 **Figure 7:** Mud-dominated facies F2. A) Molluscan-rich peloidal packstones (F2A facies) The  
1220 thin section shows dissolution of a gastropod and the abundance of microspar cement (PPL:  
1221 plane polarized). B) Hand sample image showing the accumulation of molluscs in the facies  
1222 F2A. The molluscan assemblage is dominated by *Polymesoda sp.* (*Pol.*) and small hydrobids  
1223 (white arrow). C) Outcrop photograph showing the decimetre thick tabular beds of the mud-  
1224 dominated facies (F2). D) Thin section of the facies F2A exhibits a mould after *Polymesoda sp.*  
1225 (*Pol.*) in the upper quarters of the picture and small gastropod moulds (*Gast.*) in the lower left  
1226 and right-hand quarters and abundant microspar cementation (PPL). E) Thin section of  
1227 Characean-rich peloidal wackestone to packstone (F2B facies) displaying abundant characean  
1228 cortical cells and stems (*Char.*) and ostracods (*Ostr.*). The matrix is made of densely packed  
1229 peloids. F) Peloidal wackestone to packstones with reworked calcitic rafts (*cr*) (F2C facies). G)  
1230 Thin section (under PPL) of the facies F2D showing abundant ostracods (*Ostr.*), molds of  
1231 gastropods (*Gast.*) and (reworked?) ooids (*Oo.*). The micrite is inhomogeneous suggesting  
1232 burrowing and bioturbation. H) Hand sample image displaying molluscan-rich ostracod

1233 wackestone (F2D facies): the molluscan shells are preserved as moulds. The assemblage is  
1234 dominated by gastropods (*Gast.*) and by the bivalve *Polymesoda* (*Pol.*).

1235 **Figure 8:** Planar-laminated bindstones (F3 facies) and pedogenic carbonate breccia (F4 facies).

1236 A) Field photograph of the southern face of the quarry displaying the vertical evolution from  
1237 the oolitic peloidal grainstones (lower white double arrow) to the brecciated interval (dark  
1238 double arrow). The red thick dashed line indicates a subaerial exposure surface, and the yellow  
1239 interval indicates few centimetres-thick oolitic grainstone. The laminated bindstones occur in  
1240 the upper part of the picture (see Fig. 8B and 8C). B) Close-up view of the planar-laminated  
1241 bindstone. Infra-centimetric pores are moulds after *Melanopsis* gastropod dissolution. C) Thin  
1242 section under plane polarized light of F3 facies displaying alternations of dark (micrite) and  
1243 light (accumulation of characean cortical cells fragments and calcite microspar) crinkled to  
1244 wavy laminae, with characean gyrogonite (*gyr.*). D-E) Microphotographs under plane polarized  
1245 light of brecciated limestones. D) Thin section showing vertical and curved cracks (root trace:  
1246 *rt*) filled with calcite. White box indicates a dissolution vug filled with calcitic pseudomorphs  
1247 after gypsum. E) Close-up view of the box in B) showing relicts of the tabular to microlenticular  
1248 gypsum and the replacing calcitic micrite to microspar. F) Thin section showing the  
1249 intrasediment growth of gypsum within the oolitic-peloidal grainstone. The similarity in  
1250 petrographic characters with the underlying F1B facies (see Fig. 8A) and the grain contact  
1251 points to post-depositional gypsum growth after lake evaporation. The Alizarine Red staining  
1252 in red colors indicates calcite mineralogy (plane polarized light). G) close-up view showing  
1253 calcite pseudomorphs after gypsum that occupy the inter-oolidal space.

1254 **Figure 9:** Composite log of the butte Iouton succession compiling the depositional textures, the  
1255 lithofacies stacking pattern, the interpreted transgressive-regressive (T-R) cycles, carbonate  
1256 grain composition of limestones after point-counting on thin-sections, the relative abundance

1257 of selected preserved biota,  $\delta^{18}\text{O}$  and  $\delta^{13}\text{C}$  vertical changes and estimated salinity domains.  
1258 See Figure 2 for detailed legend.

1259 **Figure 10:** Carbon and oxygen stable isotopes results. A)  $\delta^{18}\text{O} - \delta^{13}\text{C}$  cross-plot for all samples  
1260 ( $n = 58$ ): the labels refer to the lithofacies (see text for further detail). The Priabonian marine  
1261 box (Veizer et al., 1999), isotope signatures of lacustrines carbonates from the Issirac basin  
1262 (Lettéron et al., 2017) as well as interpretations of factors controlling  $\delta^{18}\text{O} - \delta^{13}\text{C}$  trends are  
1263 reported. B-C-D)  $\delta^{18}\text{O} - \delta^{13}\text{C}$  cross-plot for cycles U1 (B), U2 (C), U3 (D) and U4-U5 (E) with  
1264 samples labelled as a function of lithofacies. Isotope values are expressed in per mil (‰) and  
1265 are relative to V-PDB.

1266 **Figure 11:** Depositional model for the late Priabonian saline lake margin from butte Iouton.

1267 **Figure 12:** Palaeogeographical reconstruction of saline lakes from Languedoc and southern  
1268 Rhône valley during the late Priabonian. The siliciclastic fluxes are compiled from the previous  
1269 studies: Lettéron et al. (2022) for the Célas sandstones from Sommières and ASCI systems, and  
1270 Cavalier et al. (1984) for the plausible late Eocene to early Oligocene siliciclastic infill of the  
1271 Vistrenque basin.

1272

### 1273 **Table caption**

1274 **Table 1:** Facies classification of the Butte Iouton limestones: biological contents, sedimentary  
1275 and diagenetic features, and their paleoenvironmental interpretations.

1276 **Table 2:** Carbon and Oxygen isotope ratio, diagenetic features and lithofacies of measured  
1277 samples.

1278

# Figure 01

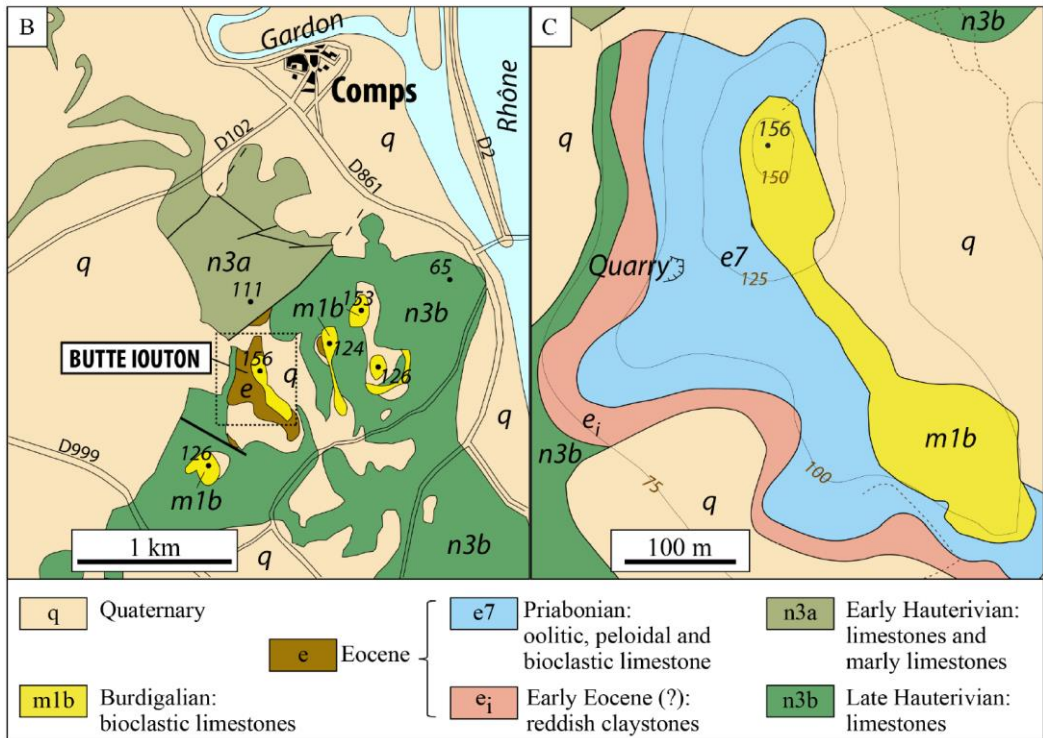
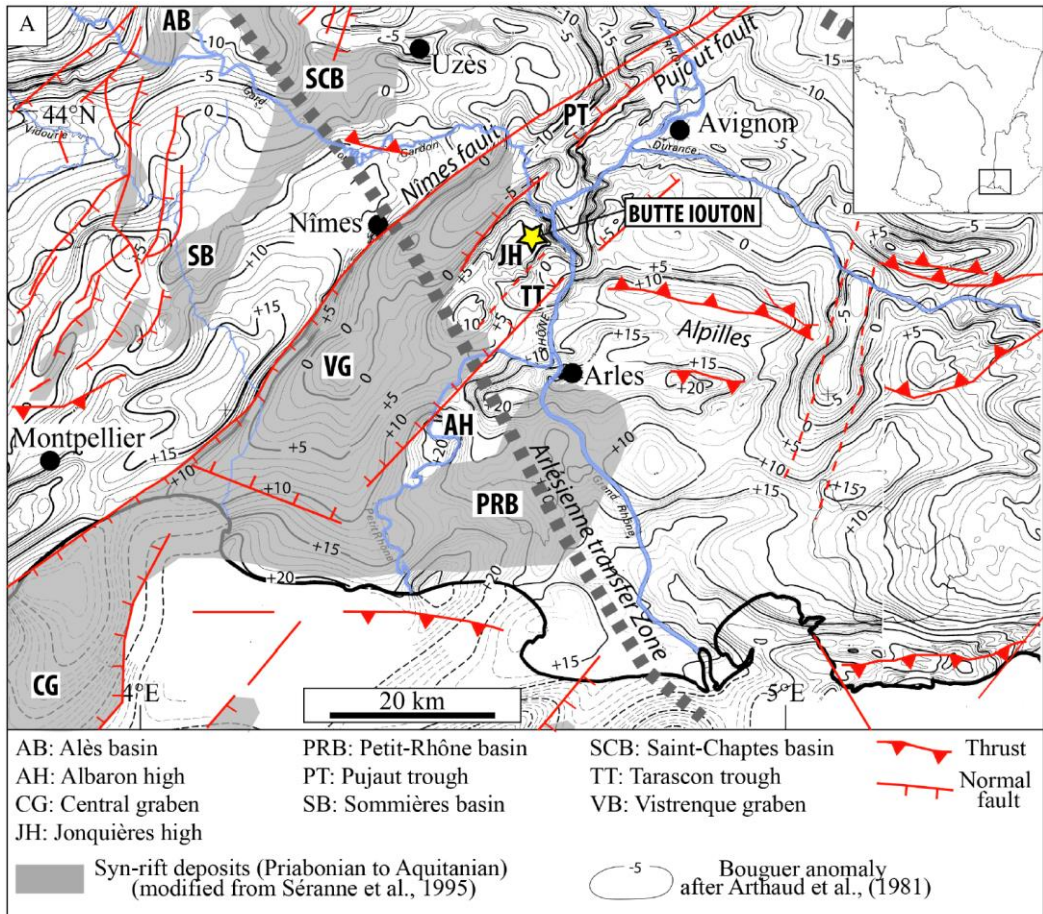


# Figure 02

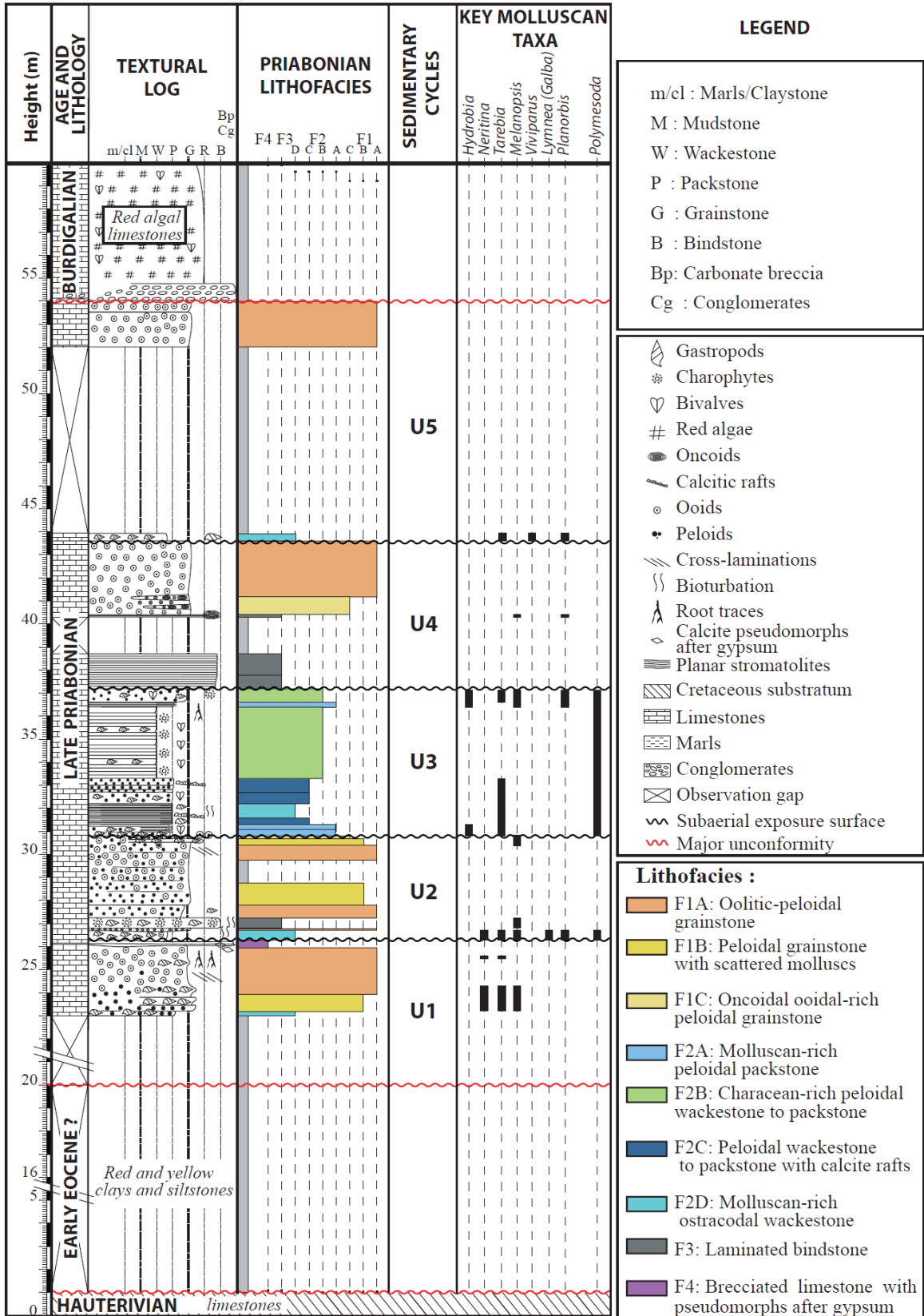


Figure 03

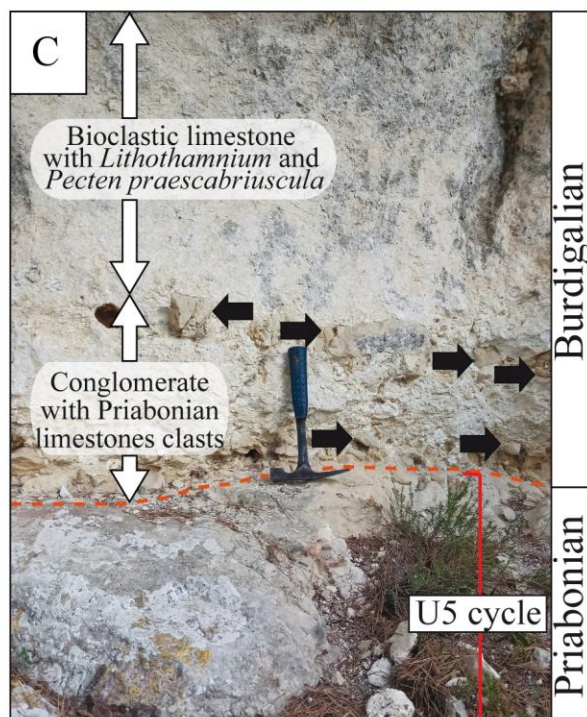
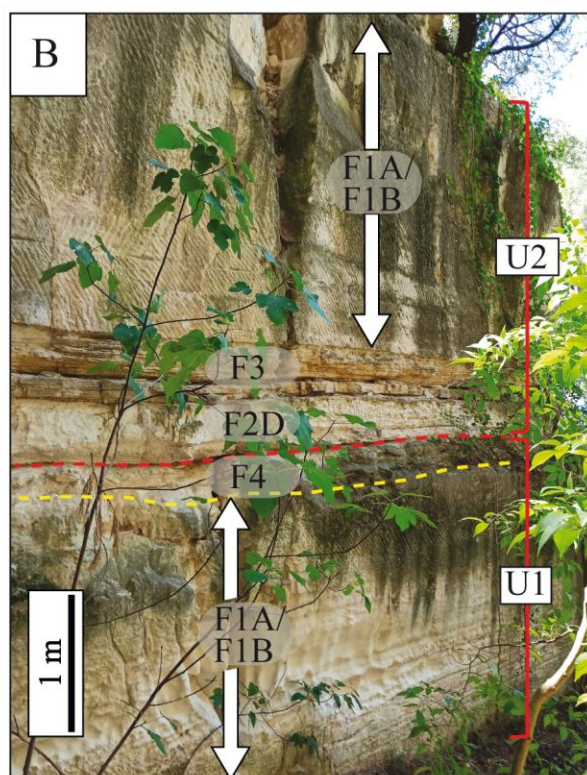
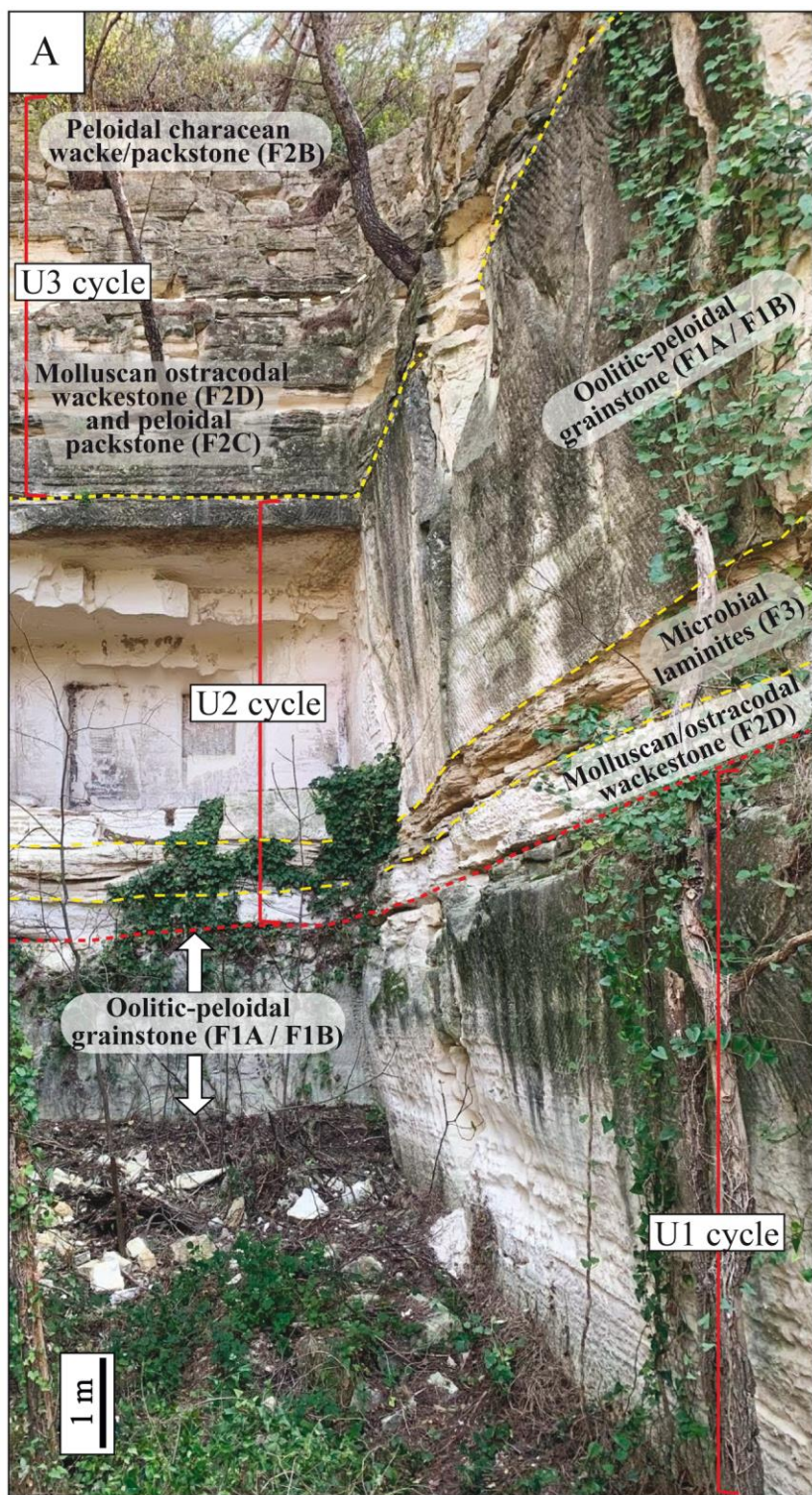


Figure 04

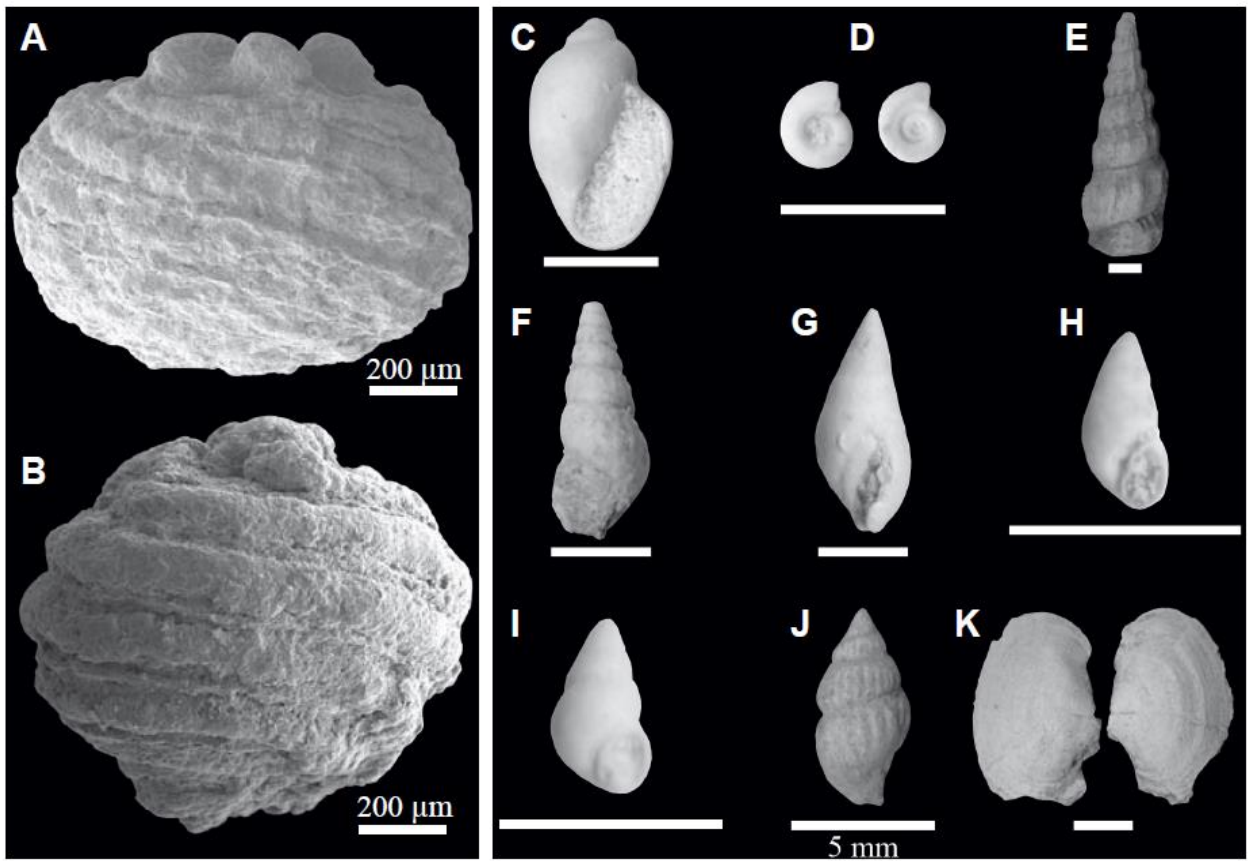


Figure 05

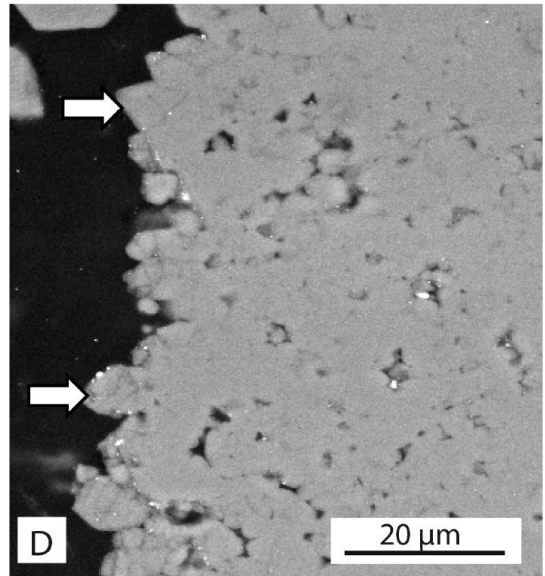
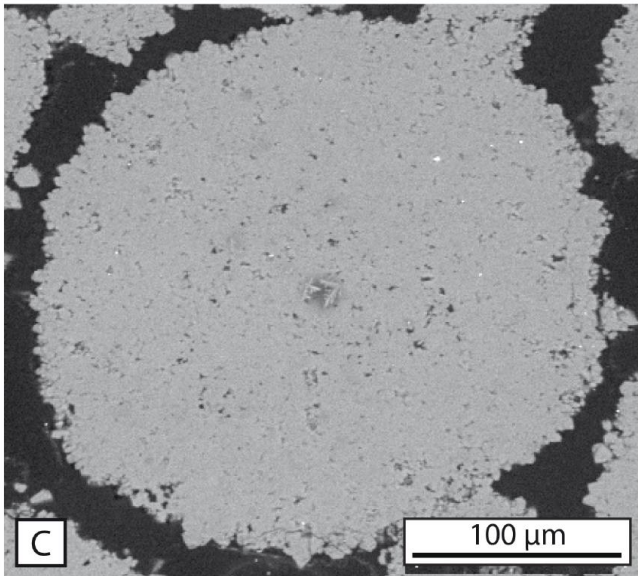
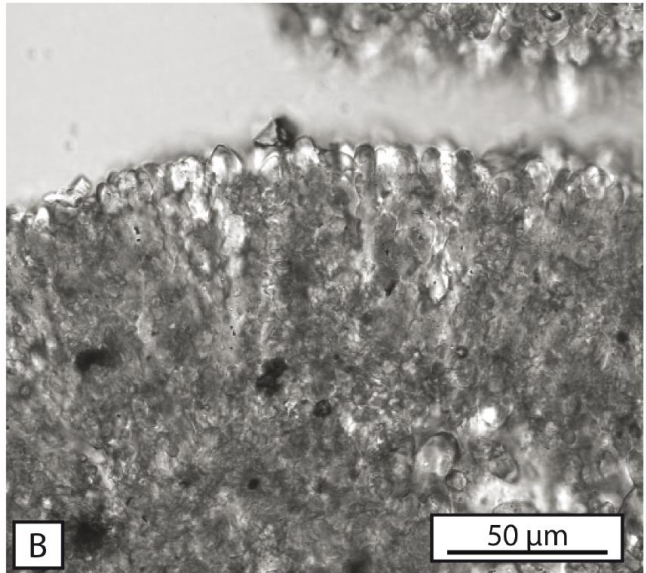
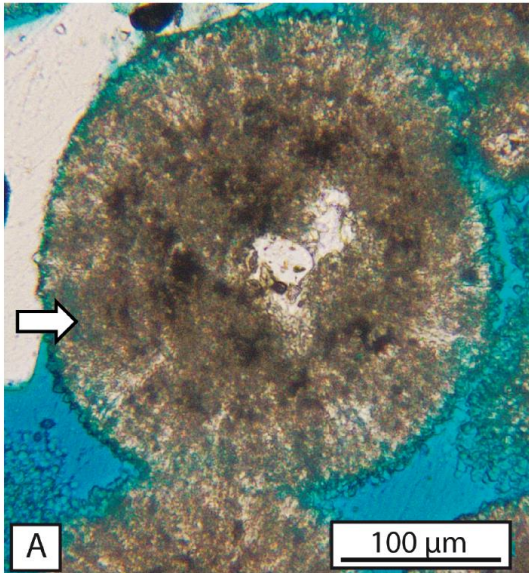


Figure 06

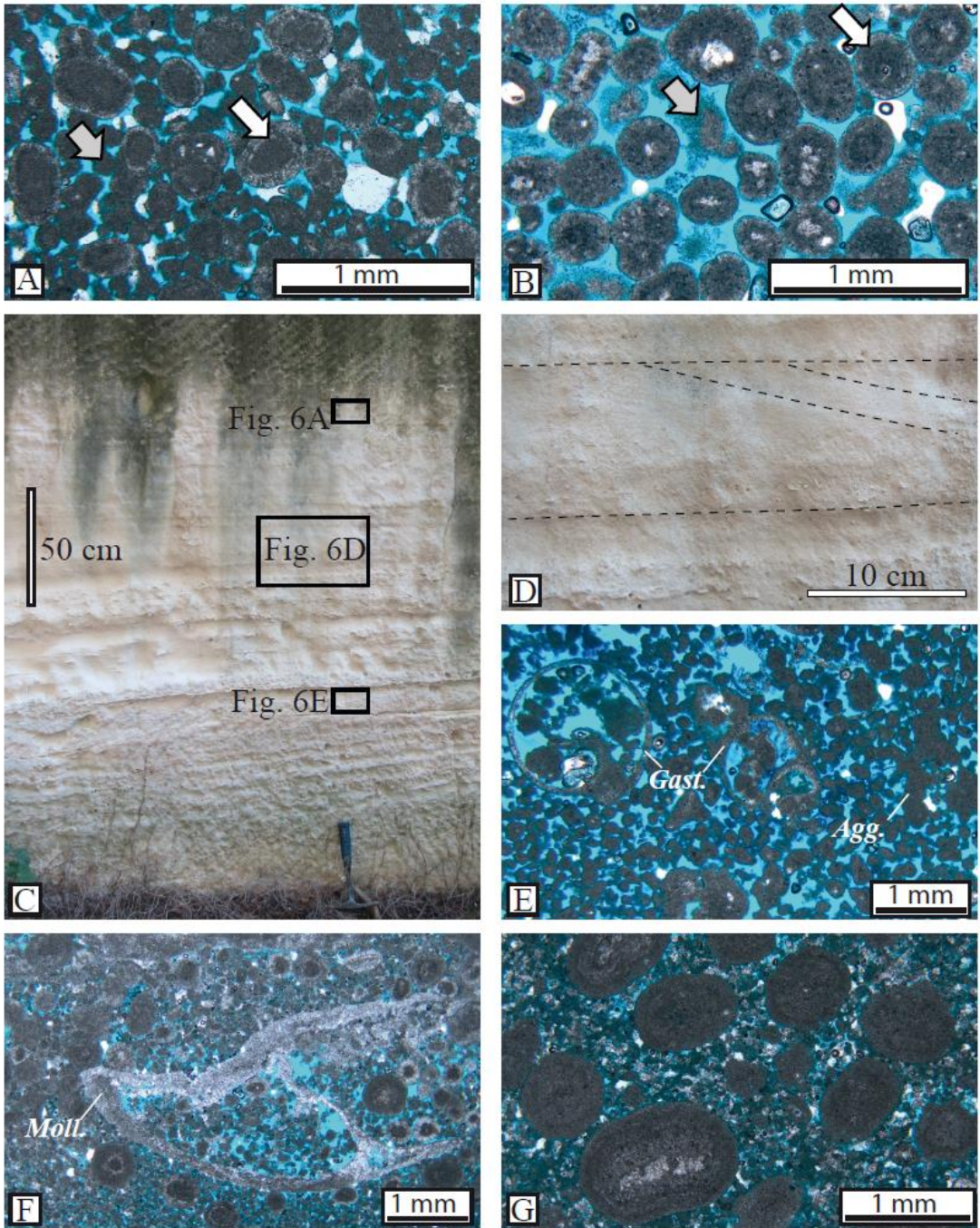


Figure 07

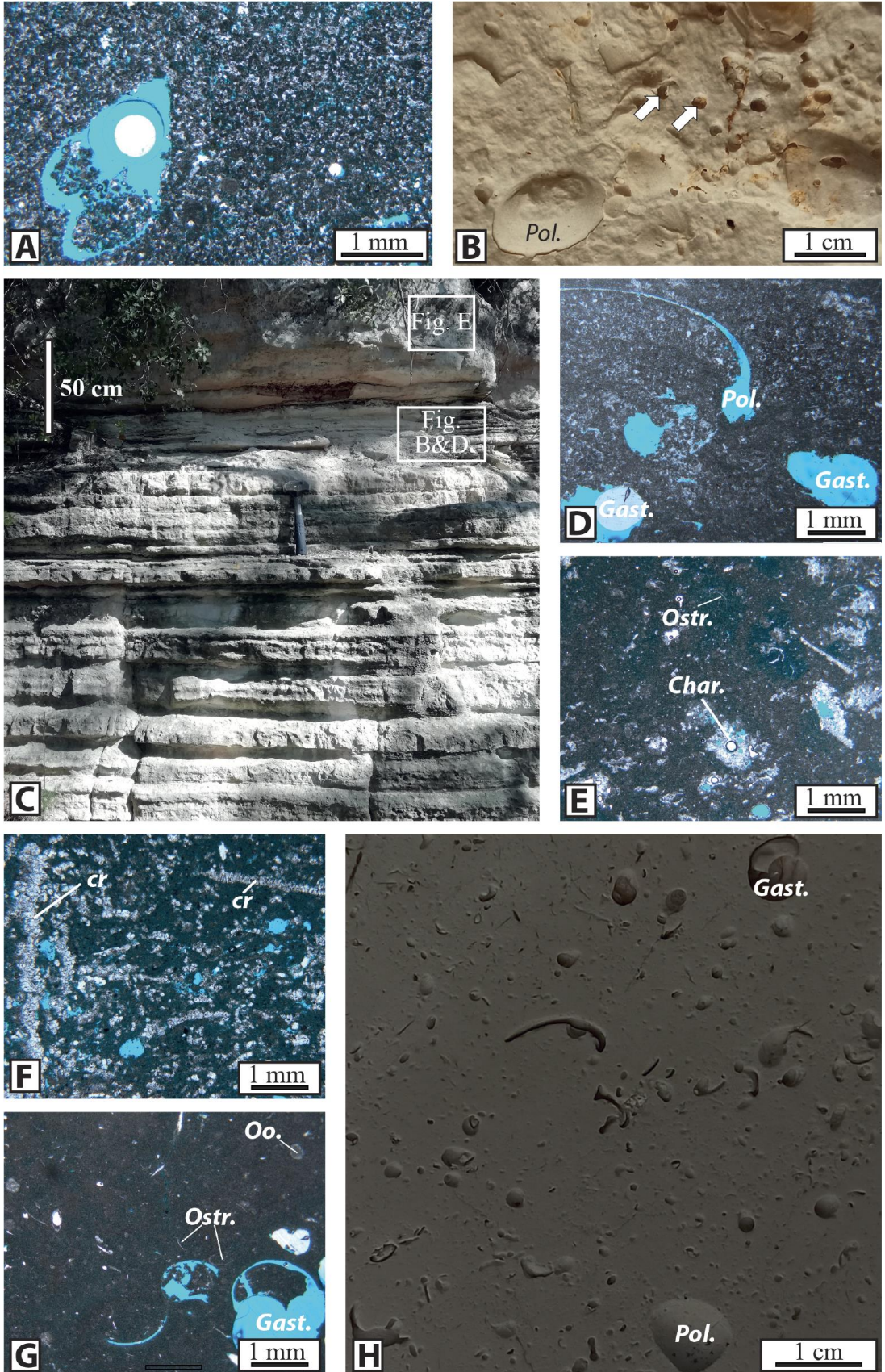
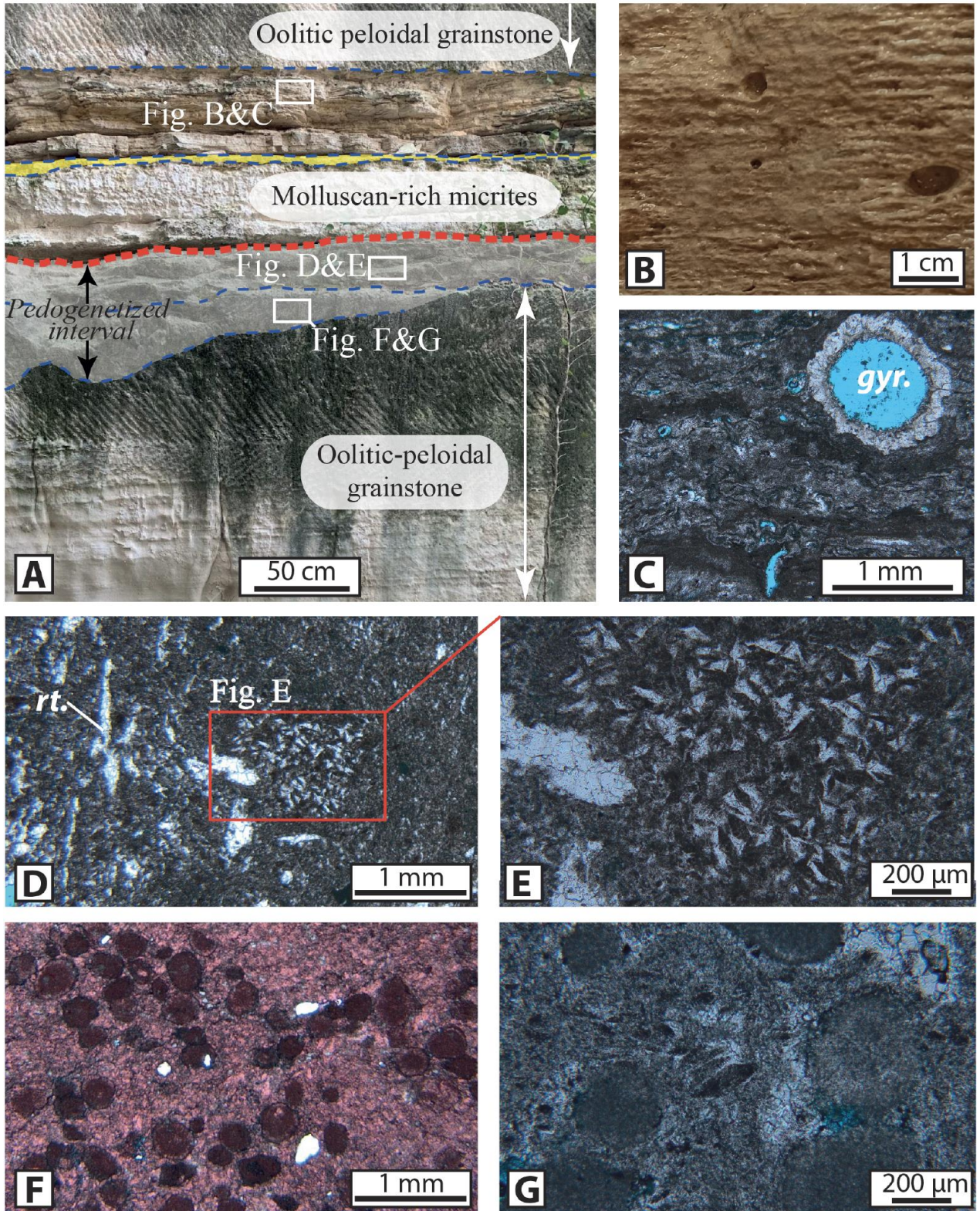
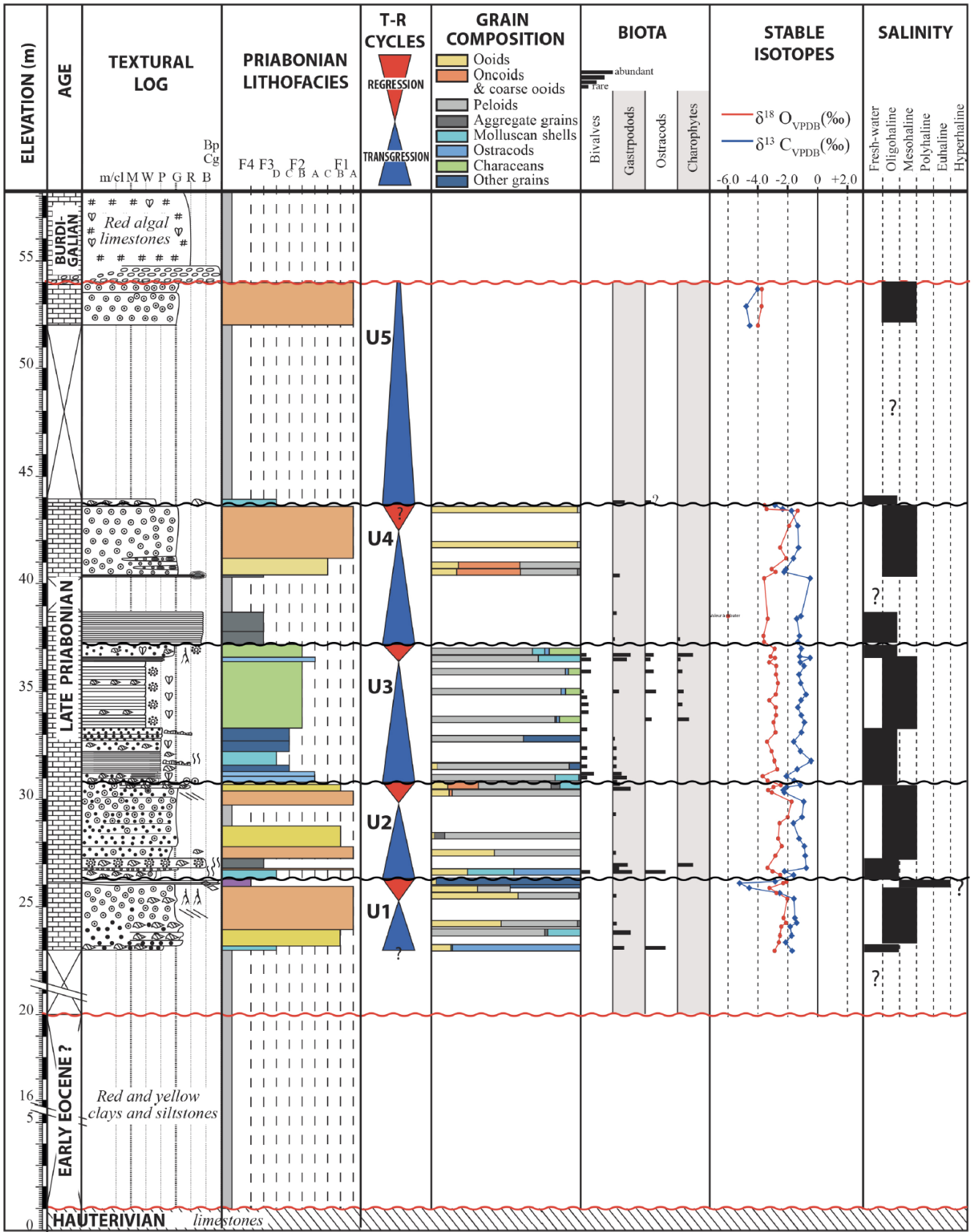


Figure 08



# Figure 09



# Figure 10

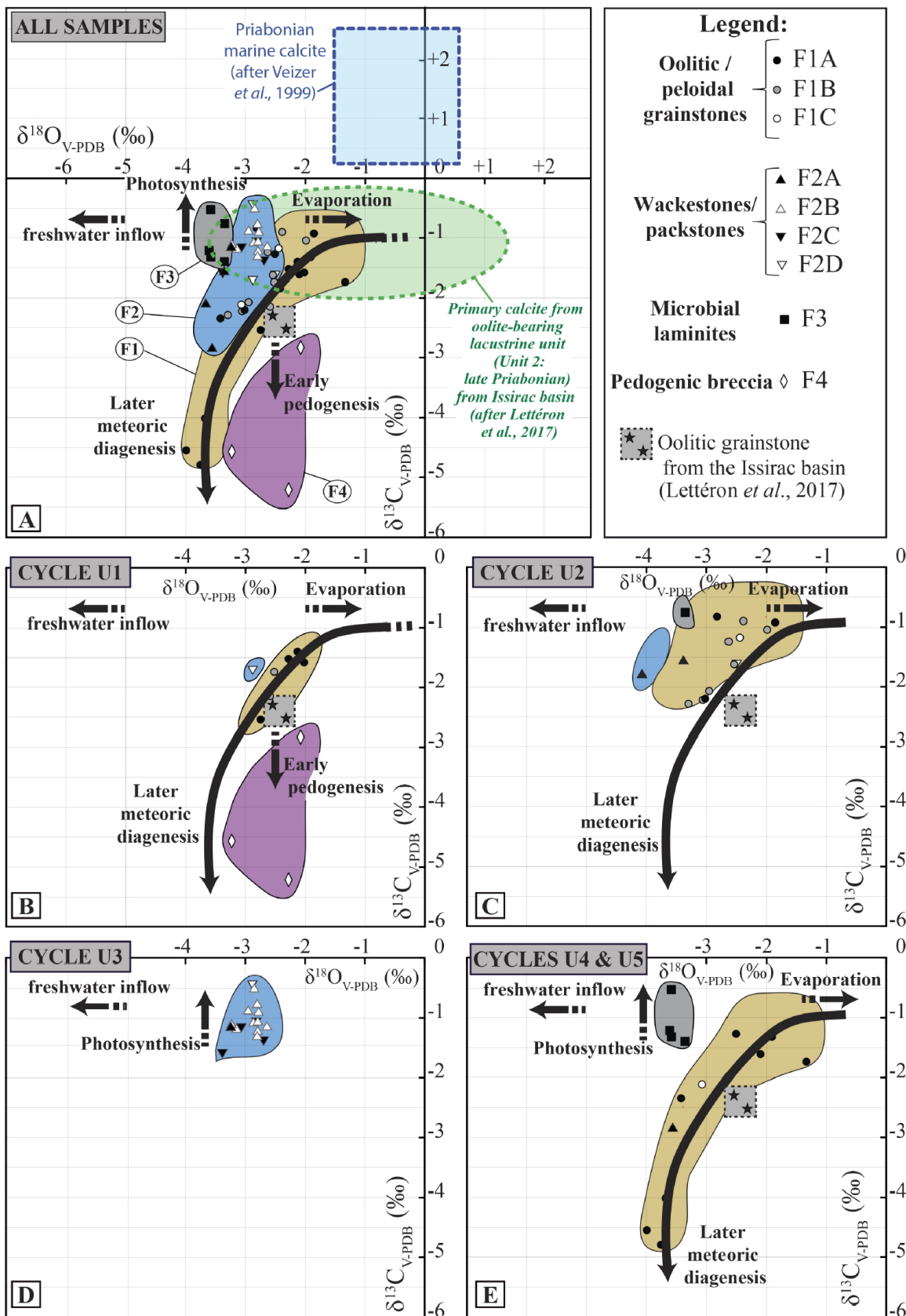
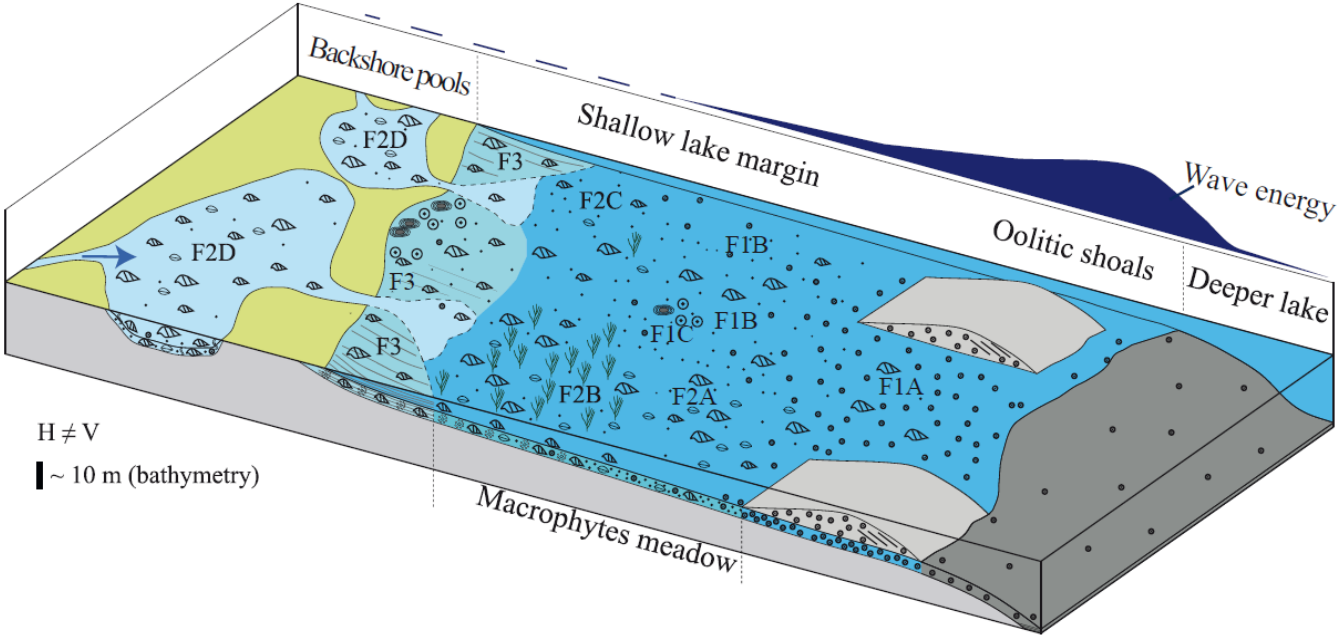
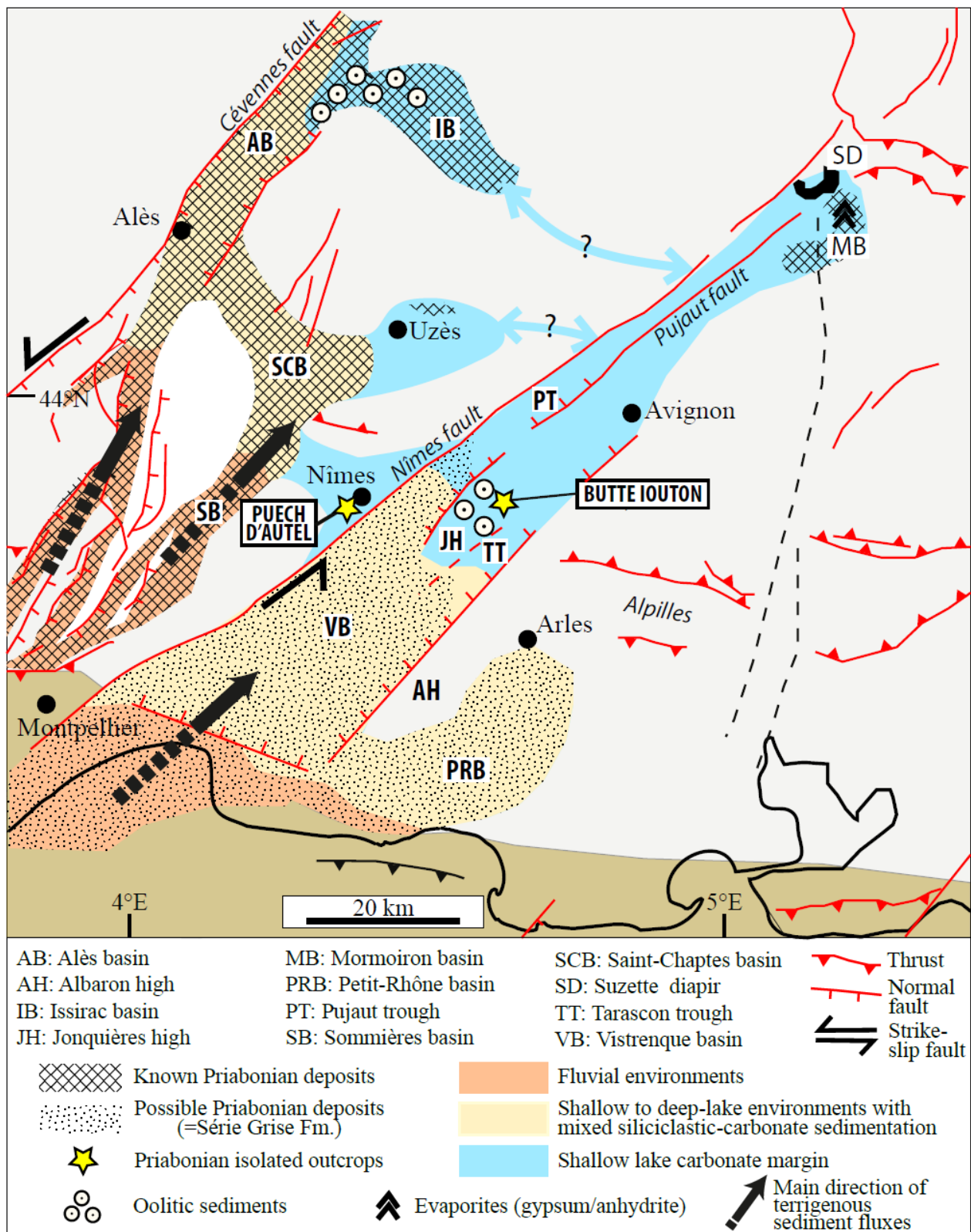


**Figure 11**



- |  |                                  |  |                      |  |                           |
|--|----------------------------------|--|----------------------|--|---------------------------|
|  | Gastropods                       |  | Planar stromatolites |  | Pseudomorphs after gypsum |
|  | Bivalves                         |  | Oncoids              |  | Bioturbation              |
|  | Ostracods                        |  | Ooids                |  | Cross bedding             |
|  | Charophyte leaving plants        |  | Peloids              |  |                           |
|  | Charophyte stems and gyrogonites |  |                      |  |                           |

Figure 12



	<b>Facies</b>	<b>Dominant biota</b>	<b>Sedimentary structures</b>	<b>Stratal pattern</b>	<b>Diagenetic features</b>	<b>Paleoenvironmental interpretation</b>
<b>F1A</b>	Oolitic-peloidal grainstone	Gastropods : <i>Melanopsis</i> , <i>Tarebia</i> , <i>Neritina</i> .	Seldom visible cross-stratifications. Good sorting (unimodal) to bimodal distribution.	Massive, can form up to 2-3 metres thick units with peloidal rich grainstones (F1B)	- Micritization of shells and ooids cortices -Intragranular microporosity development - Microrhombic micrite overgrowths -Minor compaction features at grain contact	Moderate to high energy, shallow, oligo-mesohaline , perennial lake environments, at the vicinity of oolitic shoals.
<b>F1B</b>	Peloidal grainstone	Gastropods : <i>Melanopsis</i> , <i>Tarebia</i> , <i>Neritina</i> .	Seldom visible cross-stratifications. Bimodal distribution of the grains.	Massive, can form up to 2-3 metres thick units with oolitic-rich grainstones (F1A)	- Micritization of shells and ooids cortices --Intragranular microporosity development -Minor compaction features at grain contact	Moderate energy, shallow, oligo-mesohaline, perennial lake environments, in backshoal setting.
<b>F1C</b>	Oncoidal-oidal-peloidal grainstone	Scarce gastropods	Gravel lenses of coarse-sized grains	Centimetre-thick strata	- Micritization of shells and ooids cortices -Intragranular microporosity development -Minor compaction features at grain contact	Moderate to high energy, shallow, oligo-mesohaline , perennial lake environments. .
<b>F2A</b>	Mollusk-rich peloidal packstone-grainstone	Bivalves (Polymesoda), gastropods (Hydrobids, <i>Tarebia</i> ), ostracods, scarce charophytes	Structureless	Few centimetres to decimetre tabular beds	- Microsparry and sparry calcite cements - dissolution of molluscan shells	Shallow, oligo-mesohaline lake with low to moderate water energy.
<b>F2B</b>	Characean-rich peloidal wackestone-packstone	Characean gyrogonites and stems, ostracods, mollusks ( <i>Polymesoda</i> ,	Structureless	Centimeter-thick tabular to nearly horizontal beds forming up to 4 m thick set of platelets	- Dissolution of aragonitic shells -Microsparry to sparry calcite cements in molds	Shallow, perennial oligo-mesohaline lake with Characean meadows

<b>F2C</b>	Peloidal wackestone to packstone with calcitic rafts	<i>Tarebia</i> , hydrobids) Bivalves ( <i>Polymesoda</i> ), gastropods ( <i>Tarebia</i> )	Structureless	limestones Decimetre tabular beds	- Dissolution of aragonitic shells	Shallow, perennial oligo-mesohaline lake, within or at vicinity of unpreserved macrophyte meadows
<b>F2D</b>	Molluscan-ostracodal wackestone	Ostracods, gastropods ( <i>Lymnaea</i> , <i>Viviparus</i> , <i>Planorbis</i> , <i>Tarebia</i> )	Inhomogeneous micrite, burrowing and bioturbation	Decimetre tabular beds to metre beds	- Dissolution of aragonitic shells	Low energy, shallow freshwater to oligohaline pools and sheltered areas of the lake margin.
<b>F3</b>	Planar-laminated bindstone	Characean gyrogonites and stems, ostracods, gastropods (mainly <i>Melanopsis</i> )	Alternation of subhorizontal to wavy and crinkled millimeter-thick micritic and microsparitic laminae	Up to 2 m-thick intervals of massive to platy limestones	- Dissolution of aragonitic shells -Microsparry to sparry calcite cements in molds	Low energy, very shallow freshwater to oligohaline lake margin.
<b>F4</b>	Carbonate breccia with pseudomorphs after gypsum	No preserved biota	Structureless	Decimetre thick tightly cemented and irregularly bedded limestone. Gradual transition with underlying oolitic grainstone	- Circumgranular cracks -Dissolution vug and conduits formations - Root traces - Intrasediment growth of microlenticular gypsum - Calcite pseudomorphs after gypsum - Sparry calcite cements	Paleosoil in evaporitic setting

**Table 1:** Facies classification of the Butte Iouton limestones: biological contents, sedimentary and diagenetic features, and their paleoenvironmental interpretations.

Table 2: Carbon and Oxygen isotope ratio, signal preservation vs alteration and depositional facies.

Height (m)	$\delta^{13}\text{C}$ (‰ V-PDB)	$\delta^{18}\text{O}$ (‰ V-PDB)	Diagenetic features (macroscopic and/or thin-section observations)	Depositional facies
53,8	-4,01	-3,68	Grain micritization/ microporosity	F1A
53	-4,79	-3,76	Grain micritization/ microporosity	F1A
52,1	-4,55	-3,99	Grain micritization/ microporosity	F1A
43,8	-2,83	-3,56	Grain micritization/ microporosity	F2D
43,6	-2,34	-3,42	Grain micritization/ microporosity	F1A
43,5	-1,74	-1,33	Grain micritization/ microporosity	F1A
42,8	-1,32	-1,91	Grain micritization/ microporosity	F1A
41,8	-1,27	-2,51	Grain micritization/ microporosity	F1A
41,3	-1,61	-2,11	Grain micritization/ microporosity	F1A
40,8	-2,11	-3,07	Grain micritization/ microporosity	F1C
40,65	-2,24	-2,81	Grain micritization/ microporosity	F1C
40,35	-0,53	-3,58	-	F3
38,5	-1,40	-3,35	-	F3
37,7	-1,21	-3,61	-	F3
37,4	-1,32	-3,58	-	F3
37,1	-1,08	-2,86	-	F2B
36,75	-1,20	-3,14	-	F2B
36,7	-0,50	-2,85	Primary	F2B
36,5	-1,16	-3,24	Rare calcite microspar cements	F2A
36,3	-0,90	-2,78	-	F2B
35,9	-1,24	-2,79	Rare calcite microspar cements	F2B
35,5	-1,14	-2,64	-	F2B
35	-0,78	-2,80	Rare calcite microspar cements	F2B
34,7	-1,12	-3,23	-	F2B
34,4	-1,32	-2,80	-	F2B
34	-1,08	-2,79	-	F2B
33,7	-0,88	-2,95	-	F2B
33,2	-1,07	-2,81	-	F2C
32,8	-1,59	-3,38	-	F2C
32,3	-1,15	-3,07	-	F2C
31,9	-0,43	-2,88	-	F2D
31,5	-1,37	-2,70	-	F2C
31,2	-2,09	-3,66	Microspar cements	F2A
31	-1,57	-3,35	Microspar cements	F2A
30,75	-1,17	-2,45	Grain micritization/ microporosity	F1C
30,7	-2,07	-2,95	Microspar cements	F1B
30,55	-2,29	-3,30	Grain micritization/ microporosity	F1B
30,45	-2,22	-3,06	Grain micritization/ microporosity	F1B
30	-0,92	-1,86	Grain micritization/ microporosity	F1A
29,3	-1,04	-1,99	Grain micritization/ microporosity	F1B
29	-1,62	-2,54	Grain micritization/ microporosity	F1B
28,3	-1,24	-2,63	Grain micritization/ microporosity	F1B

27,9	-0,86	-2,39	Grain micritization/ microporosity	F1B
27,5	-0,83	-2,82	Grain micritization/ microporosity	F1A
26,95	-0,76	-3,35	-	F3
26,75	-2,21	-3,02	Grain micritization/ microporosity	F1A
26,6	-1,60	-2,50	-	F2D
26,3	-2,83	-2,08	Pedogenic features/ sparry calcite cements	F4
26,2	-5,21	-2,28	Pedogenic features/ sparry calcite cements	F4
26	-4,57	-3,23	Pedogenic features/ sparry calcite cements	F4
25,75	-2,54	-2,74	Grain micritization/ microporosity	F1A
25,5	-1,58	-2,02	Grain micritization/ microporosity	F1A
24,6	-1,52	-2,28	Grain micritization/ microporosity	F1A
24,35	-1,40	-2,13	Grain micritization/ microporosity	F1A
24,2	-1,84	-2,42	Grain micritization/ microporosity	F1A
23,8	-1,73	-2,52	Grain micritization/ microporosity	F1B
23,5	-2,15	-2,59	Grain micritization/ microporosity	F1B
23,1	-1,70	-2,87	-	F2D